# CHAPTER 5

# RESULTS AND DISCUSSION (PART II):

# Lead Magnesium Niobate (PMN)

In analogouse to the PZT previously reported, synthesis, formation and characterisation of PMN powders and ceramics were performed and discussed in details here. Similar B-site preparation technique was also applied to the preparation of PMN powder. The firing conditions were also optimised by varying calcination temperatures, dwell times and heating/cooling rates. Phase formation and morphology of both MN and PMN calcined powders were studied. Then, the densification, phase analysis, microstructure and dielectric properties of sintered PMN ceramics were also investigated by XRD, SEM and dielectric measurements.

## 5.1 Magnesium Niobate Powder

### 5.1.1 Thermal Analysis

The DTA curve obtained for a powder mixed in the stoichiometric proportions of $MgNb_2O_6$ is shown in Fig. 5.1. In the temperature range from room temperature to ~ 400 $^oC$, the sample shows both exothermic and endothermic peaks, which may be attributed to the decomposition of organic species from the milling process.[110, 111] Moreover, another exothermic and endothermic peaks at ~ 500 $^oC$ and ~ 630 $^oC$ were also observed in this DTA profile, respectively. It is to be noted that there is no

obvious interpretation of these peaks, although it is likely to correspond to the solid-state reaction between MgO and $Nb_2O_5$ reported by a number of researchers.[19, 60] These data were used to define the range of temperatures (500 to 1100 $^oC$) for XRD investigation.

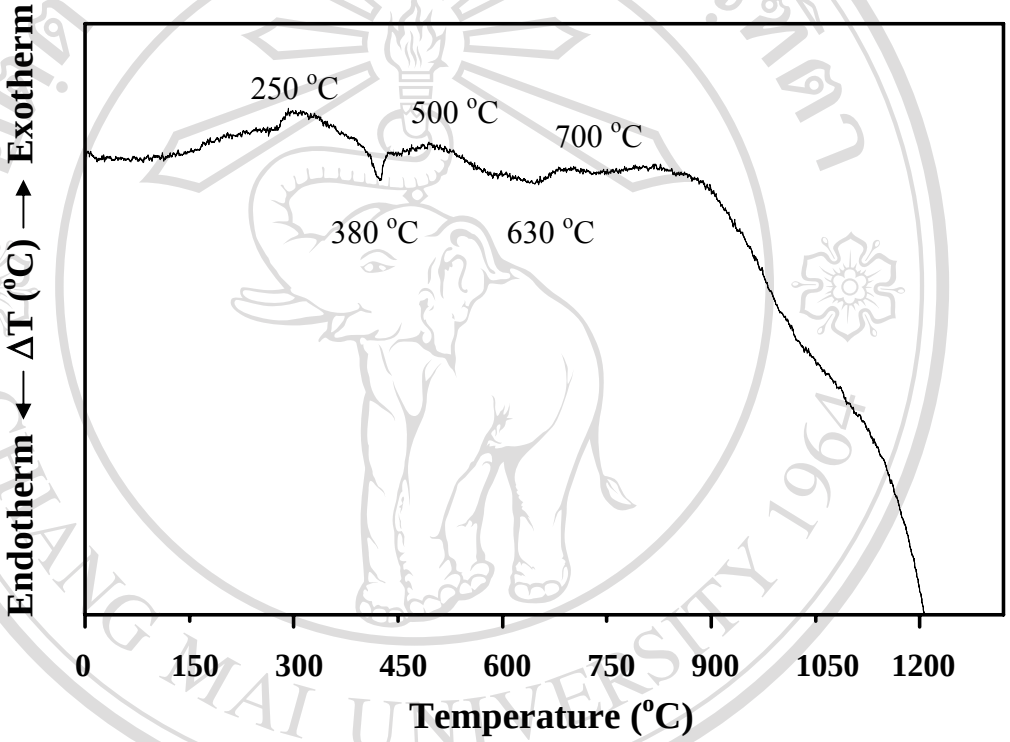


**Fig. 5.1** A DTA curve for the mixture of MgO-$Nb_2O_5$ powders.



### 5.1.2 Phase Analysis

All calcined powders, together with that of the starting powder mixtures were examined by XRD in order to investigate the phase development (Figs. 5.2-5.5). As shown in Fig. 5.2, for the starting powder, only X-ray peaks of precursors MgO (+) and $Nb_2O_5$ (*), which could be matched with JCPDS file no. 45-946[115] and 27-1312[116], respectively, are present, indicating that no reaction had yet been triggered

during the milling process. After calcination at 500 $^{o}$C, little crystalline phase of $MgNb_2O_6$ (▼) was developed, which is seen by presence of some small peak at 2θ ~ 24.35$^{o}$, 30.31$^{o}$, 31.35$^{o}$, 40.61$^{o}$ and 41.11$^{o}$ accompanying with unreacted precursors MgO and $Nb_2O_5$ as separated phases. This observation agrees well with those derived from the DTA results and other workers.[110, 111] As the temperature increased to 650 $^{o}$C, the intensity of the columbite-like $MgNb_2O_6$ peaks was further enhanced. Upon calcination at temperatures ranging from 700 to 1000 $^{o}$C, the $MgNb_2O_6$ phase became the predominant phase. It should be noted that after calcination at 800 $^{o}$C, the peak corresponding to MgO disappeared (not detectable), while the traces of minor phases of unreacted $Nb_2O_5$ could not be completely eliminated. Above 1000 $^{o}$C, a single phase of $MgNb_2O_6$ is formed, revealing that MgO has completely reacted with $Nb_2O_5$ phase. The XRD pattern of this major phase was indexable according to an orthorhombic columbite-type structure with lattice parameters $a$ = 570 pm, $b$ = 141.9 pm and $c$ = 503 pm, space group *Pcan* (no. 60), matched with JCPDS file no. 33-875 [117] and literature.[118-120]

In conventional mixed oxide route reported earlier,[118, 121, 122] the major phase of $MgNb_2O_6$ was obtained for a calcination temperature above 1100 $^{o}$C. However, for the present work, there are no significant different between the powders calcined at temperature ranging from 1050 to 1100 $^{o}$C (Fig. 5.2).

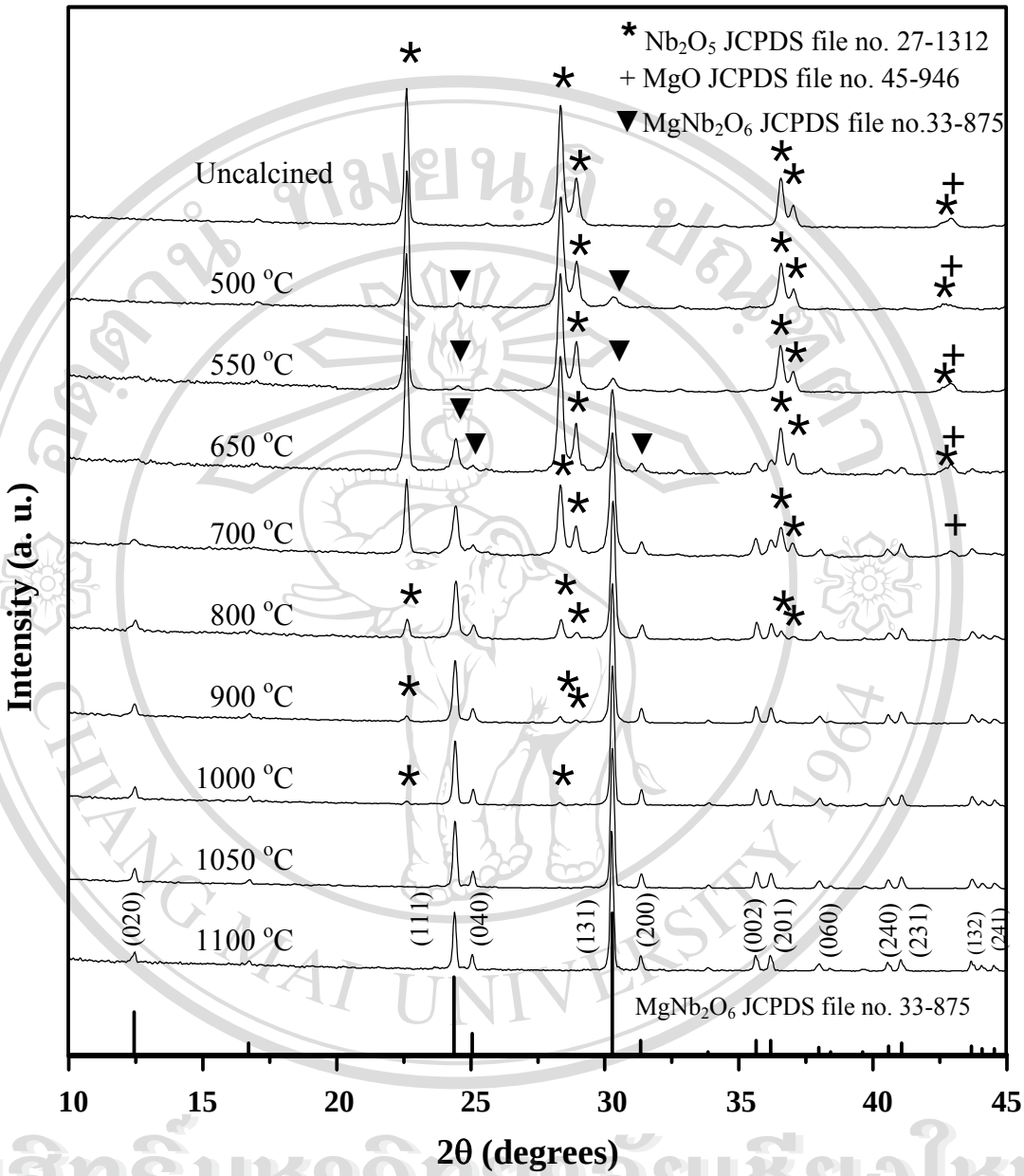


**Fig. 5.2** XRD patterns of MN powder calcined at various temperatures for 2 h with heating/cooling rates of 10 °C/min.

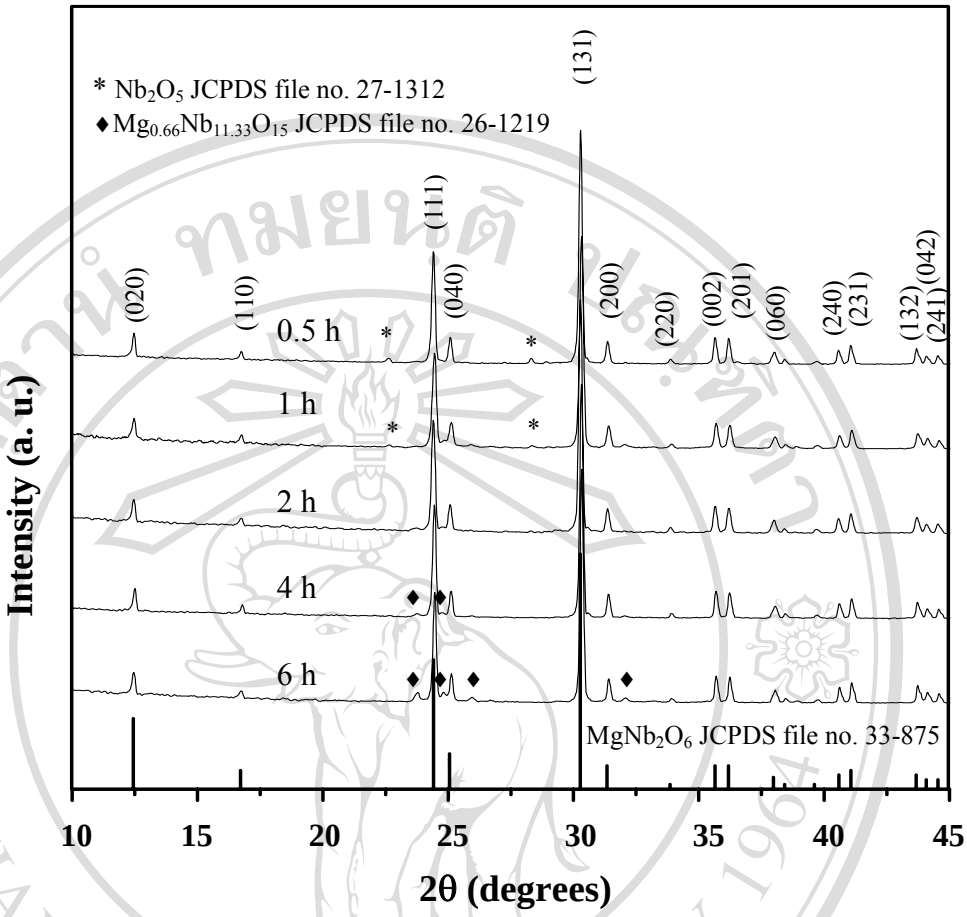


**Fig. 5.3** XRD patterns of the powders calcined at 1050 $^{o}$C with heating/cooling rates of 10 $^{o}$C/min for various dwell times.

Having established the optimum calcination temperature, alternative dwell times ranging from 0.5 h to 6 h with constant heating/cooling rates of 10 $^{o}$C/min were applied at 1050 $^{o}$C, as shown in Fig. 5.3. It is observed that the single phase of $MgNb_2O_6$ (yield of 100% within the limitations of the XRD technique) was found to be possible only in powders, calcined at 1050 $^{o}$C with dwell time of 2 h. In earlier work,[63, 119, 123] long heat treatments at ~ 1100-1300 $^{o}$C for 6, 20 and 48 h were proposed for the formation of $MgNb_2O_6$ by a conventional mixed oxide synthetic route, although no details on phase formation were provided. Saha et al.[63] have also

reported their attempts to prepare solid-state-derived $MgNb_2O_6$ powder via the introduction of re-grinding and re-calcination processes. However, in the present study, it was found that there are some extra peaks appeared (indicated by ♦) at relatively longer calcination time. This was representing the development of secondary phase, $Mg_{0.66}Nb_{11.33}O_{15}$, which could be matched with JCPDS file no. 26-1219 (Fig. 5.4). Moreover, it is clear that an essentially monophasic $MgNb_2O_6$ of columbite structure was already obtained when the calcination time was extended to 2 h without any introduction of pre-firing and remixing processes.

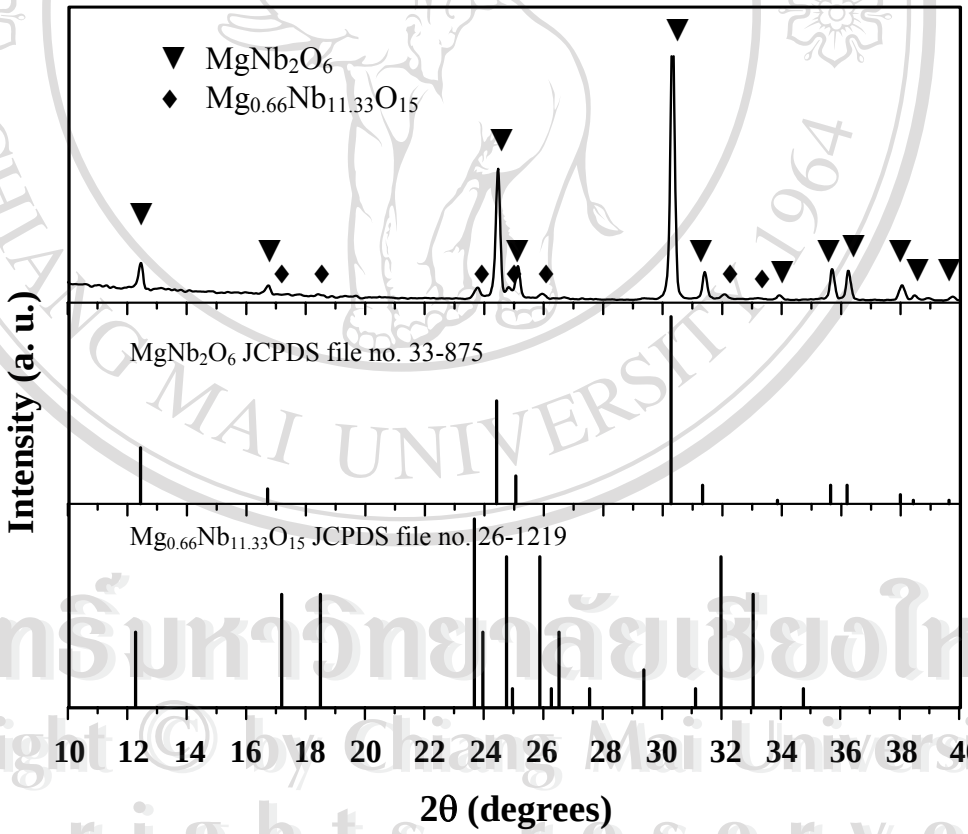




**Fig. 5.4** Computerised JCPDS data-matching confirms that formation of both $MgNb_2O_6$ and $Mg_{0.66}Nb_{11.33}O_{15}$ phases in the powder calcined at 1050 $^oC$ for 6 h with heating/cooling rates of 10 $^oC$/min.

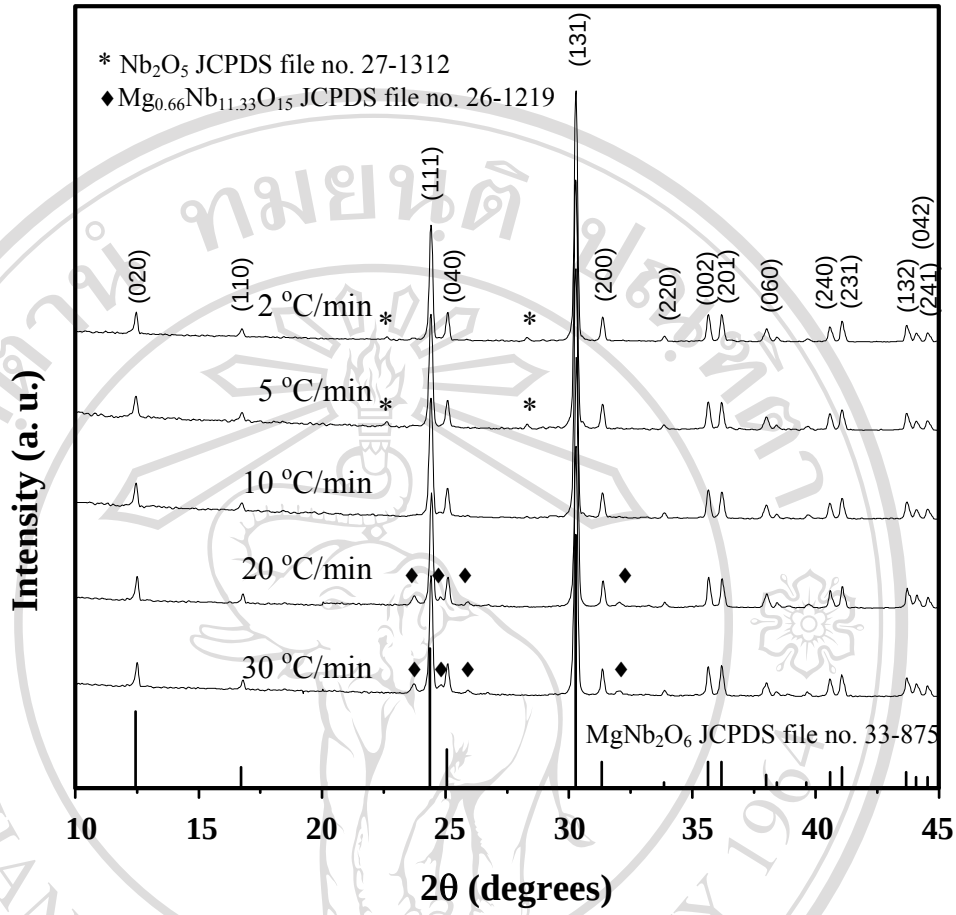


**Fig. 5.5** XRD patterns of the powders calcined at 1050 °C for 2 h with various heating/cooling rates.

To further study the phase development with increasing heating/cooling rates in the powders, an attempt was also made to calcine MN powders under various heating/cooling rates (Fig. 5.5). In this connection, it is shown that the yield of $MgNb_2O_6$ phase varies significantly with heating/cooling rates (ranging from 2 to 30 °C/min). The presence of some small amount of minor phase $Nb_2O_5$ (*) was found in the samples sintered with slow heating/cooling rates whilst $Mg_{0.66}Nb_{11.33}O_{15}$ (♦) phase was observed in the samples sintered with fast heating/cooling rates.

Based on the DTA and XRD data, it may be concluded that, over a wide range of calcination conditions, single-phase $MgNb_2O_6$ cannot be straightforwardly formed via a solid-state mixed oxide synthetic route. For purposes of estimating the concentrations of $MgNb_2O_6$ phase present, Eq. (3.5) has been applied to the diffraction patterns obtained (Table 5.1). It is well documented that powder prepared by a conventional mixed oxide method have spatial fluctuations in their compositions. The extent of the fluctuation depends on the characteristics of the starting precursors as well as the processing schedules.[19, 118, 119] It is rather surprising that no evidence of the corundum $Mg_4Nb_2O_9$[120, 121, 124] was found in this study, nor was there any indication of the $Mg_5Nb_4O_{19}$[19] being present. The experimental work carried out here suggests that the optimal calcination condition for single phase $MgNb_2O_6$ (with impurities undetected by XRD technique) is 1050 $^oC$ for 2 h with heating/cooling rates of 10 $^oC$/min. Moreover, the formation temperature and dwell time for $MgNb_2O_6$ observed in this work are also lower than those reported earlier.[19, 119, 121, 125]

**Table 5.1** Calculated MN powders as a function of calcination conditions.

| Calcination conditions | | | Qualitative concentrations of MN phase | | |
|---|---|---|---|---|---|
| Temperature ($^oC$) | Time (h) | Rates ($^oC$/min) | $Nb_2O_5$ | $MgNb_2O_6$ | $Mg_{0.66}Nb_{11.33}O_{15}$ |
| 500 | 2 | 10 | * | * | * |
| 550 | 2 | 10 | * | * | * |
| 650 | 2 | 10 | * | * | * |
| 700 | 2 | 10 | * | * | * |
| 800 | 2 | 10 | 12.87 | 87.13 | 0 |
| 900 | 2 | 10 | 4.17 | 95.83 | 0 |
| 1000 | 2 | 10 | 1.65 | 98.35 | 0 |
| 1050 | 2 | 10 | 0 | 100 | 0 |
| 1100 | 2 | 10 | 0 | 100 | 0 |
| 1050 | 0.5 | 10 | 2.28 | 97.72 | 0 |
| 1050 | 1 | 10 | * | * | * |
| 1050 | 4 | 10 | 0 | 98.36 | 1.64 |
| 1050 | 6 | 10 | 0 | 95.63 | 4.37 |
| 1050 | 2 | 2 | 1.30 | 98.70 | 0 |
| 1050 | 2 | 5 | 1.65 | 98.35 | 0 |
| 1050 | 2 | 20 | 0 | 95.84 | 4.16 |
| 1050 | 2 | 30 | 0 | 96.42 | 3.58 |

* $Nb_2O_5$, $MgNb_2O_6$ and $Mg_{0.66}Nb_{11.33}O_{15}$ phases were found and Eq. (3.5) is not valid.

### 5.1.3 Morphological Analysis

The morphological changes in the $MgNb_2O_6$ powders formed by a mixed oxide method are illustrated in Fig. 5.6 as a function of calcination temperatures. The powders seem to have a similar morphology. In general, the particles are agglomerated and basically irregular in shape, with a substantial variation in particle size, particularly in samples calcined at higher temperature. The range of particle diameter was found to be about 0.08-0.28, 0.13-0.68, 0.33-1.18 and 0.36-1.22 μm for the samples calcined at 800, 1000, 1050 and 1100 $^{o}$C, respectively. The results indicate that averaged particle size and degree of agglomeration tend to increase with calcination temperatures. The morphology–calcination relationship of $MgNb_2O_6$ powders prepared by the solid-state reaction observed here tend to have a similar features compared with the previous report.[118]

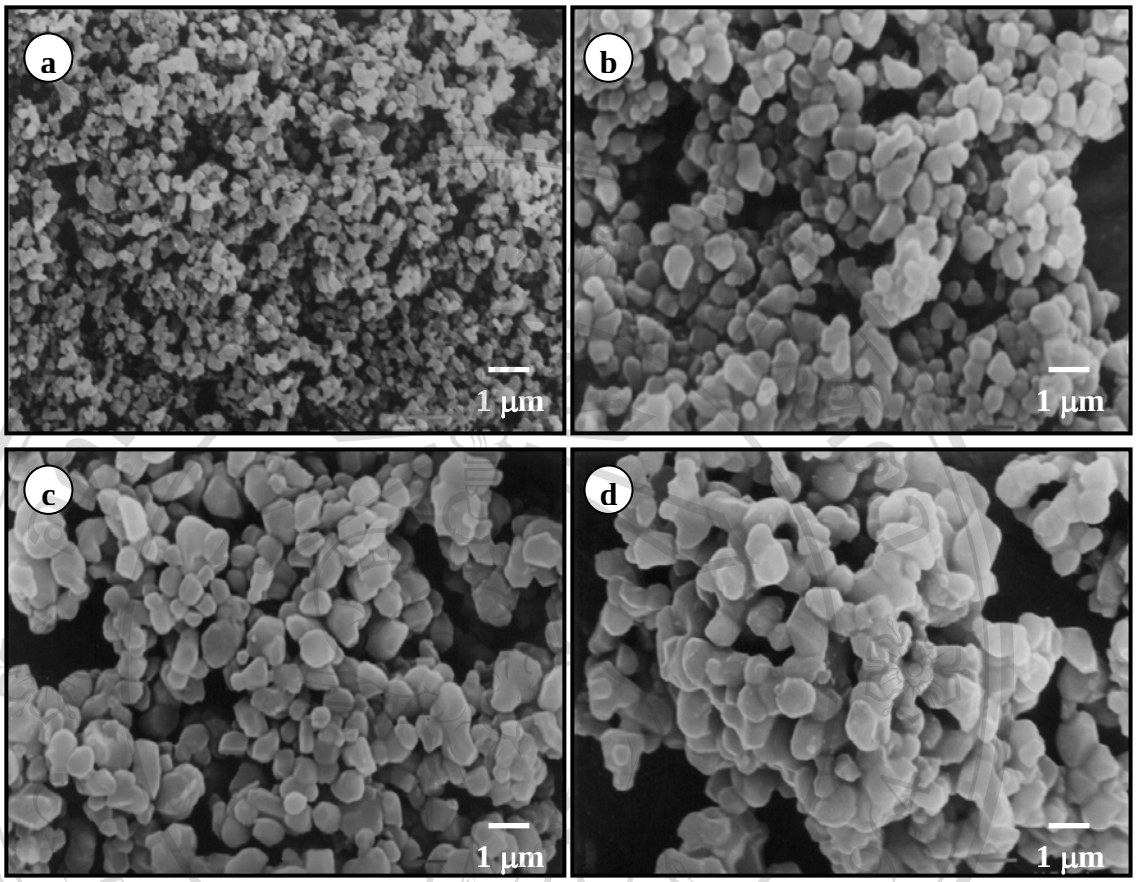


**Fig. 5.6** SEM micrographs of the MN powders calcined at (a) 800 $^{o}$C, (b) 1000 $^{o}$C, (c) 1050 $^{o}$C and (d) 1100 $^{o}$C, all for 2 h with heating/cooling rates of 10 $^{o}$C/min.

## 5.2 Lead Magnesium Niobate Powder

Having prepared the single-phase $MgNb_2O_6$ powder, a mixed oxide synthetic route was developed for the preparation of PMN powder. In this study, the formation of perovskite phase, morphology and particle size of the calcined PMN powders have been investigated as a function of calcination conditions by TG-DTA, XRD and SEM techniques.

### 5.2.1. Thermal Analysis

The result of TG-DTA simultaneous analysis of a powder mixed in the stoichiometric proportions of $Pb(Mg_{1/3}Nb_{2/3})O_3$ is shown in Fig. 5.7. It is seen that the TG curve demonstrates two distinct weight losses. In the temperature range from room temperature to ~ 320 $^oC$, both small exothermic and endothermic peaks are observed in the DTA curve in consistent with the first weight loss (~ 0.7 %). These observations can be attributed to the decomposition of the organic species from the milling process. Increasing the temperature up to ~ 1000 $^oC$, the solid-state reaction occurred between PbO and $MgNb_2O_6$.[64, 120, 125, 126] The broad exotherm in the DTA curve represents that reaction, which has a maximum at ~ 630 $^oC$. This is supported by a slightly decrease in sample weight (~ 1.9 %) observed in the TG curve. No further significant weight loss was observed for the temperatures above 500 $^oC$ in the TG-curve, indicating that the minimum firing temperature to get PbO-$MgNb_2O_6$ compounds is in good agreement with XRD result (Fig. 5.8) and those of other workers.[64, 120, 123, 125] However, the DTA curve shows that there is another endothermic peak at ~ 840 $^oC$, indicating the eutectic point of PbO.[19, 57, 62] These data were used to define the range of temperatures (600 to 1100 $^oC$) for XRD investigation.

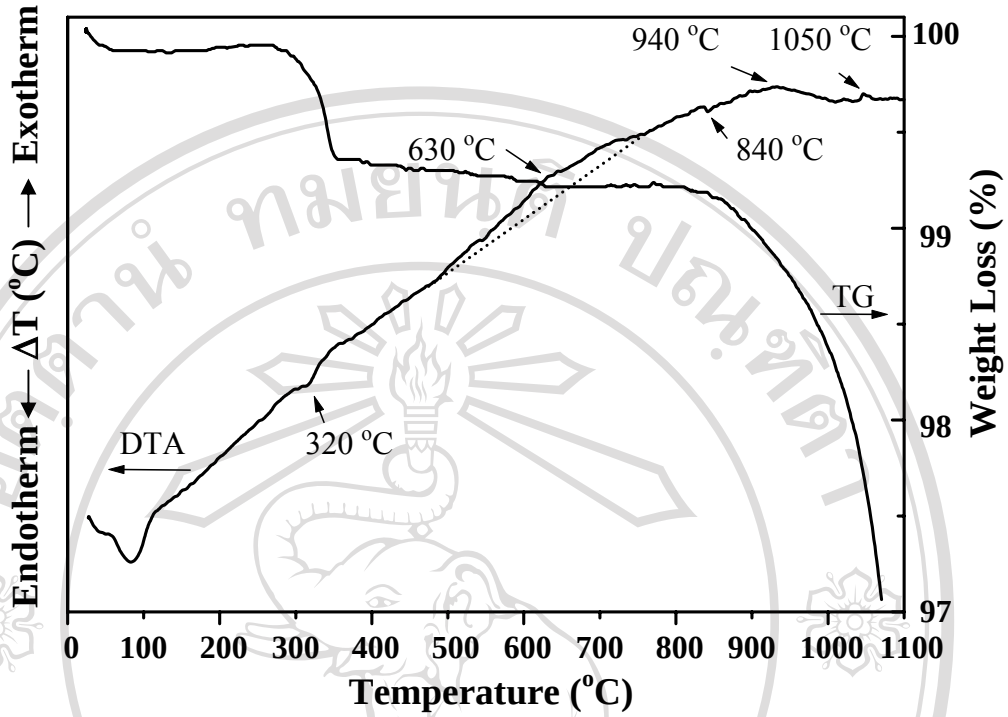


**Fig. 5.7** TG-DTA curves for the mixture of PbO-$MgNb_2O_6$ powder.

### 5.2.2 Phase Analysis

To further study the phase development in the powder with increasing calcination temperature, the powders were calcined for 2 h in air at various temperatures, up to 1100 °C, followed by phase analysis using XRD. As shown in Fig. 5.8, for the uncalcined powder, only X-ray peaks of precursors PbO (*) and $MgNb_2O_6$ (+) are present, which could be matched with JCPDS file numbers 38-1477[127] and 33-875[117], respectively. This result indicates that no reaction had yet been triggered during the milling process. After calcination at 600 °C, little crystalline phase of $Pb(Mg_{1/3}Nb_{2/3})O_3$ (∇) with (pseudo) cubic symmetry (JCPDS file no. 27-1199[128]) was developed accompanying with PbO and $MgNb_2O_6$ as separated phases. This observation agrees well with those derived from the TG-DTA results and those of

other workers.[125, 126, 129, 130] As the temperature increased to 600 $^{o}$C, the intensity of the perovskite-like $Pb(Mg_{1/3}Nb_{2/3})O_3$ peaks was further enhanced. Upon calcination at temperatures ranging from 650 to 1100 °C, the $Pb(Mg_{1/3}Nb_{2/3})O_3$ phase became the predominant phase. It should be noted that when calcination temperature exceeds 700 $^{o}$C, the peaks corresponding to PbO and $MgNb_2O_6$ disappeared (not detectable), where as the traces of unknown phases (•) were observed. In B-site precursor mixed oxide route, single phase of PMN were obtained for a calcination temperature between 700-900 $^{o}$C.[19, 62, 126] However, for the present study, there are no significant differences between the powders calcined at temperatures ranging from 700 to 1100 $^{o}$C. Further increase of the calcination temperature to 1100 $^{o}$C does not result in very much increase in the amount of PMN, whereas unknown phase (•) remains unchanged. This could be attributed to the limitation of the milling process and the different reactivities between PbO, MgO and $Nb_2O_5$.[123] It is to be noted that even for a wide range of calcination conditions, single-phase PMN cannot be produced in this work.

According to the additional peaks (•) of the unknown phase at 2θ ~ 29° and 48° observed in the XRD patterns, the possible pyrochlore phases, such as $Pb_{1.83}Nb_{1.71}Mg_{0.29}O_{6.39}$, $Pb_5Nb_4O_{15}$, $Pb_3Nb_4O_{13}$, $Pb_2Nb_2O_7$ or $Pb_3Nb_2O_8$[57, 123] can be formed. Attempt has been made to identify these unknown phases by enlarging these peaks and matching with the computerized JCPDS data of all possible phases, as shown in Fig. 5.9. It can be seen that the broad peak at 2θ ~ 29° may be seperated into two sharper peaks when calcination temperature exceed 900 °C and both peaks are well matched with the standard diffraction patterns of JCPDS file no. 33-769 and 46-637. Thus, the most possible of pyrochlore phase present in this profile may be

identified as $Pb_{1.83}Nb_{1.71}Mg_{0.29}O_{6.39}$ (JCPDS file no. 33-769). For calcination temperature above 900 °C, the $Pb_5Nb_4O_{15}$ (46-637) phase is revealed as another possible pyrochlore phase that present along with the first one. These observation may be due to the effect of liquid phase PbO during high temperature process which creates another equilibrium phase and attributed to the formation of pyrochlore phase.[57, 125, 130] According to the literature, oxygen-deficiency has been claimed to responsible for the occurrence of the pyrochlore phase with general formula of $Pb_{2-x}(Mg_{0.286}Nb_{1.714})O_{6.571-x}$ where $0 < x < 0.286$.[131]

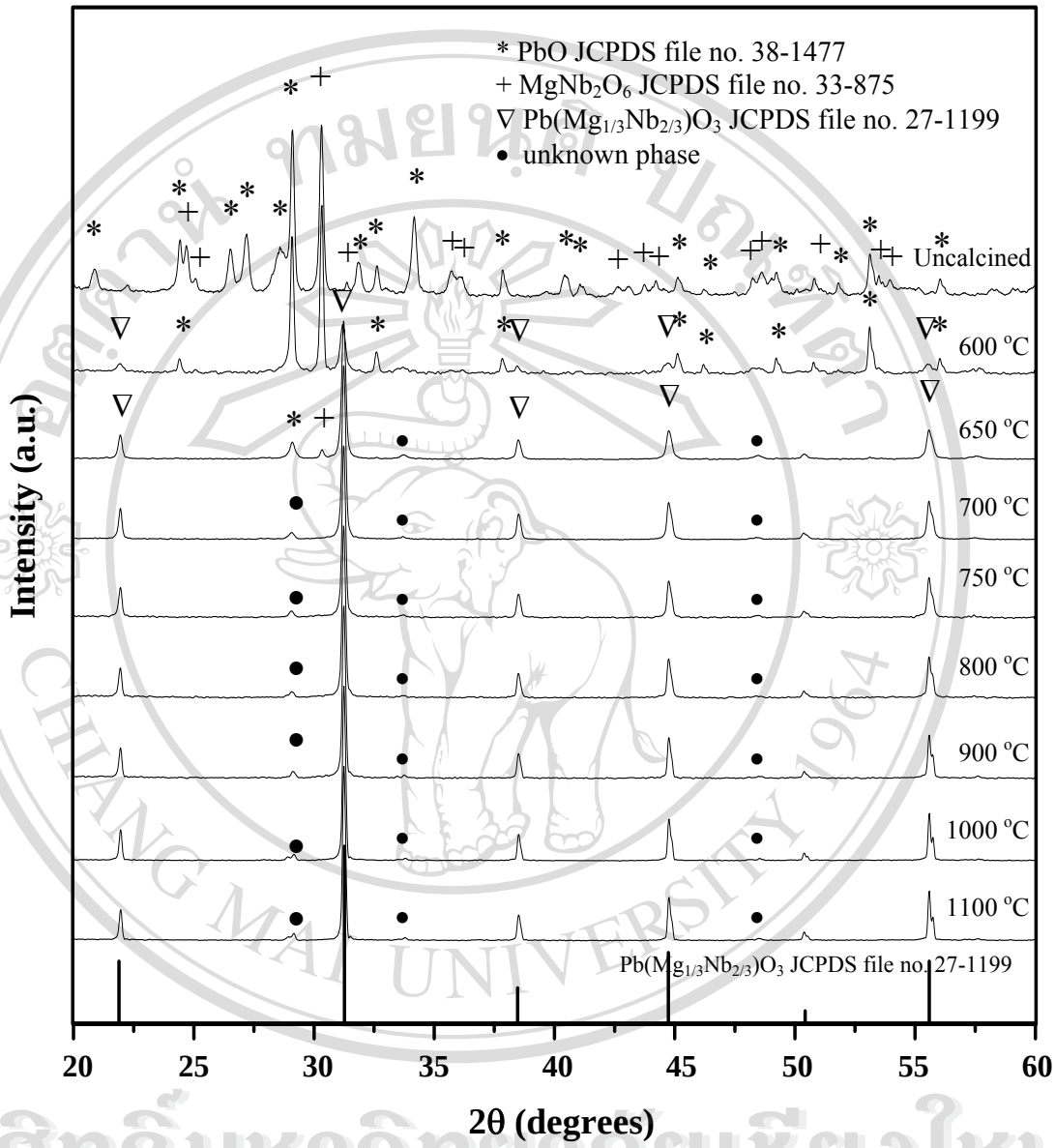


**Fig. 5.8** Powder XRD patterns of the samples calcined at various temperatures for 2 h with heating/cooling rates of 10 °C/min.

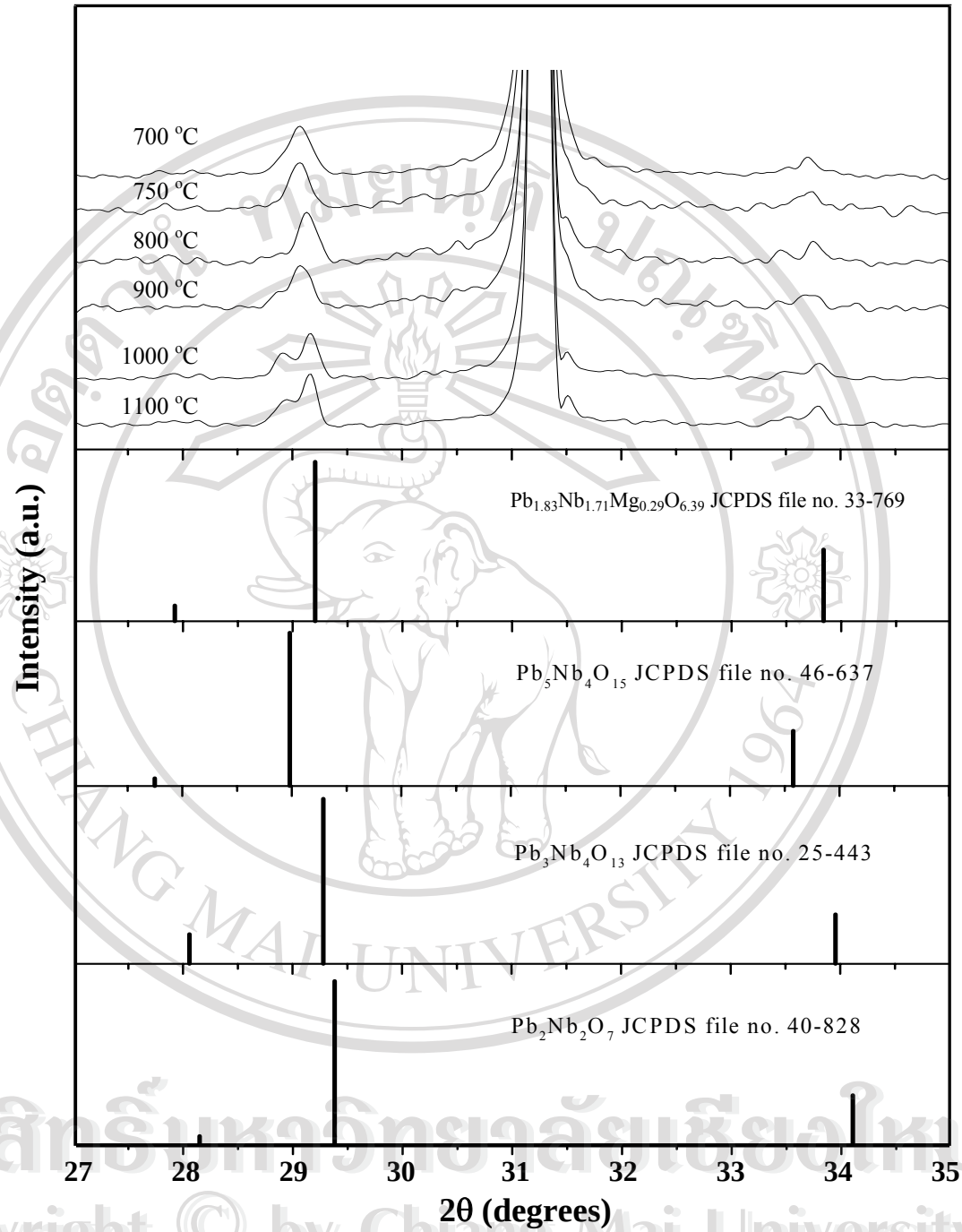


**Fig. 5.9** Computerised JCPDS data-matching indicates the possibility of peaks overlapping between $Pb_5Nb_4O_{15}$ and $Pb_{1.83}Nb_{1.71}Mg_{0.29}O_{6.39}$ phases in the powders calcined at various temperatures for 2 h with heating/cooling rates of 10 °C/min.

Apart from the calcination temperature, the effect of the dwell time and heating/cooling rates on phase formation were also studied. In the present study, it was found that there are no significant differences between the powders calcined at 750 $^{o}$C with dwell time ranging from 0.5 to 6 h (Fig. 5.10) or with heating/cooling rates ranging from 2 to 20 $^{o}$C/min (Fig. 5.11). The same pyrochlore $Pb_{1.83}Nb_{1.71}Mg_{0.29}O_{6.39}$ was found to form together with perovskite PMN in all cases.

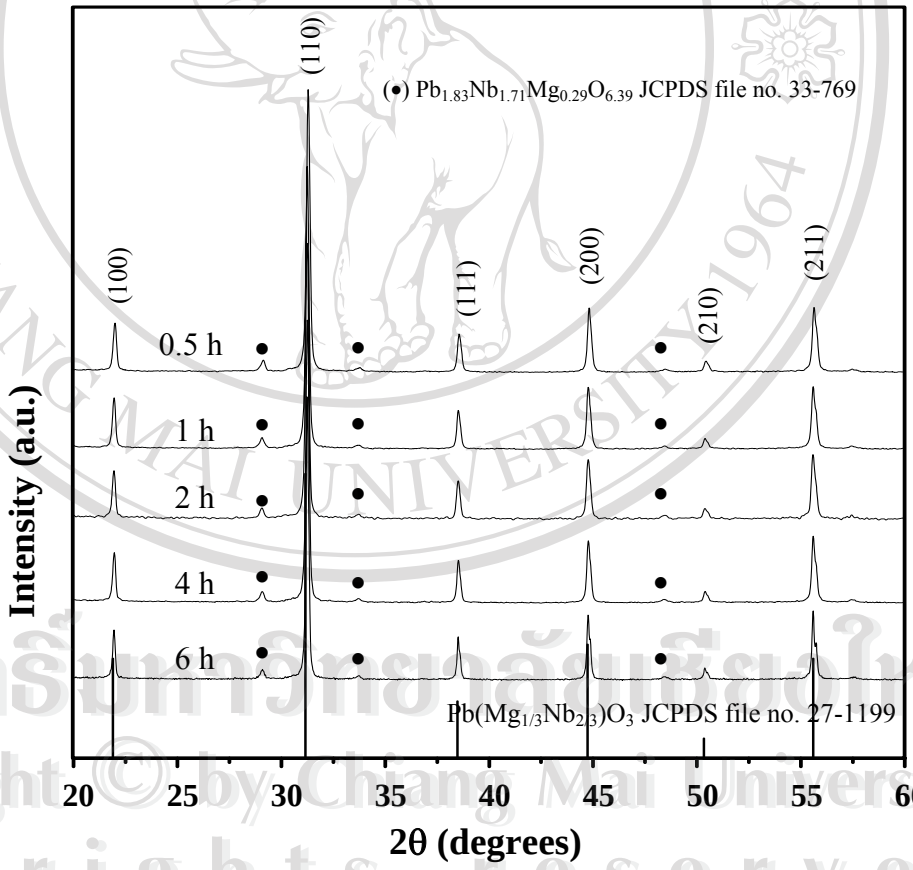




**Fig. 5.10** Powder XRD patterns of the samples calcined at 750 $^{o}$C with heating/cooling rates of 10 $^{o}$C/min for various dwell times.

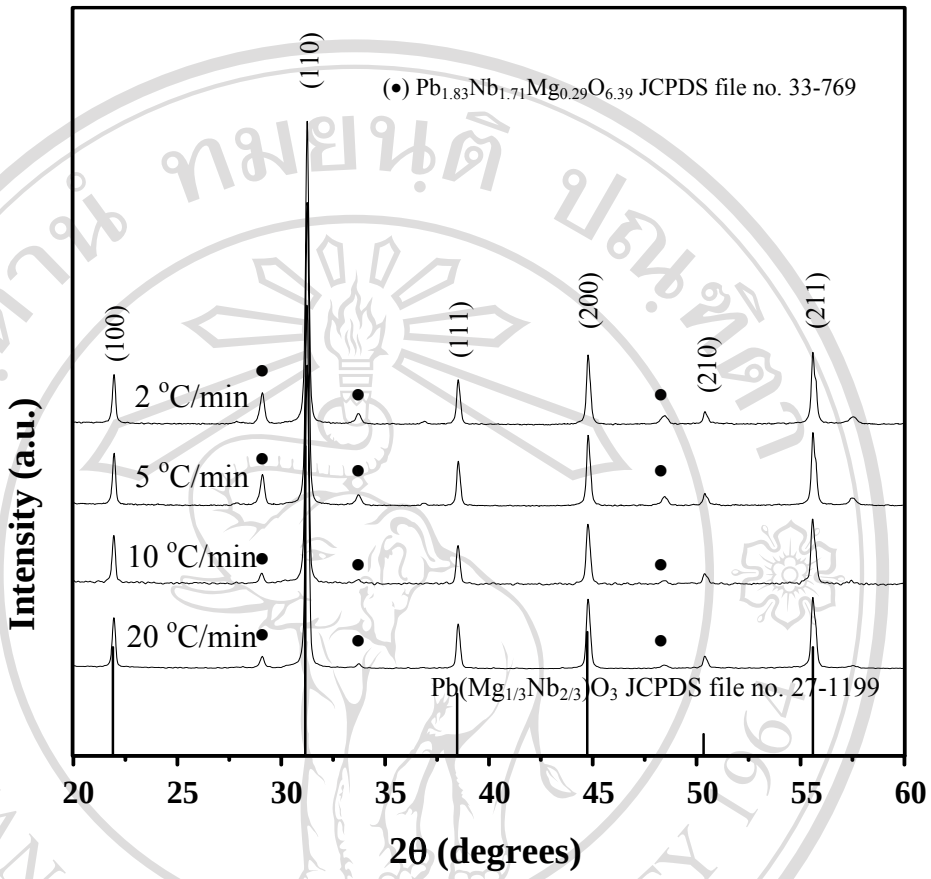


**Fig. 5.11** Powder XRD patterns of the samples calcined at 750 °C for 2 h with various heating/cooling rates.



Based on the XRD data, it may be concluded that, over a wide range of calcination conditions, single-phase PMN cannot be formed via a solid-state mixed oxide synthetic route although the columbite-$MgNb_2O_6$ precursor is used. It is well documented that powders prepared by a mixed oxide method have spacial fluctuations

in their compositions. The extent of the fluctuation depends on the characteristics of the starting precursors as well as the processing schedules.

### 5.2.3 Morphological Analysis

The morphological changes in the PMN powders formed by a mixed oxide technique are shown in Fig. 5.12 (a-e) as a function of the formation temperature. After various calcination temperatures, the powders have similar morphology. In general, they had spherical secondary particles composed of nano-sized primary particulates. The primary particles have sized ~ 100-365 nm, and the agglomerates measured ~ 0.4-1.7 μm. It is well known that this granule characteristic will offer an apparent advantage towards achieving a high sintered density and homogeneous microstructure for ceramic at a reduced sintering temperature.

According to Fig. 5.13 and table 5.2, EDS analysis from a large number of the calcined powders confirmed the parent composition to be $Pb(Mg_{1/3}Nb_{2/3})O_3$ in agreement with XRD results. A combination of SEM and EDS techniques has demonstrated that MgO-rich PMN phase (pyrochlore) exists neighbouring the PMN parent phase and points to the poor reactivity of MgO precursor in good agreement with other works.[47]

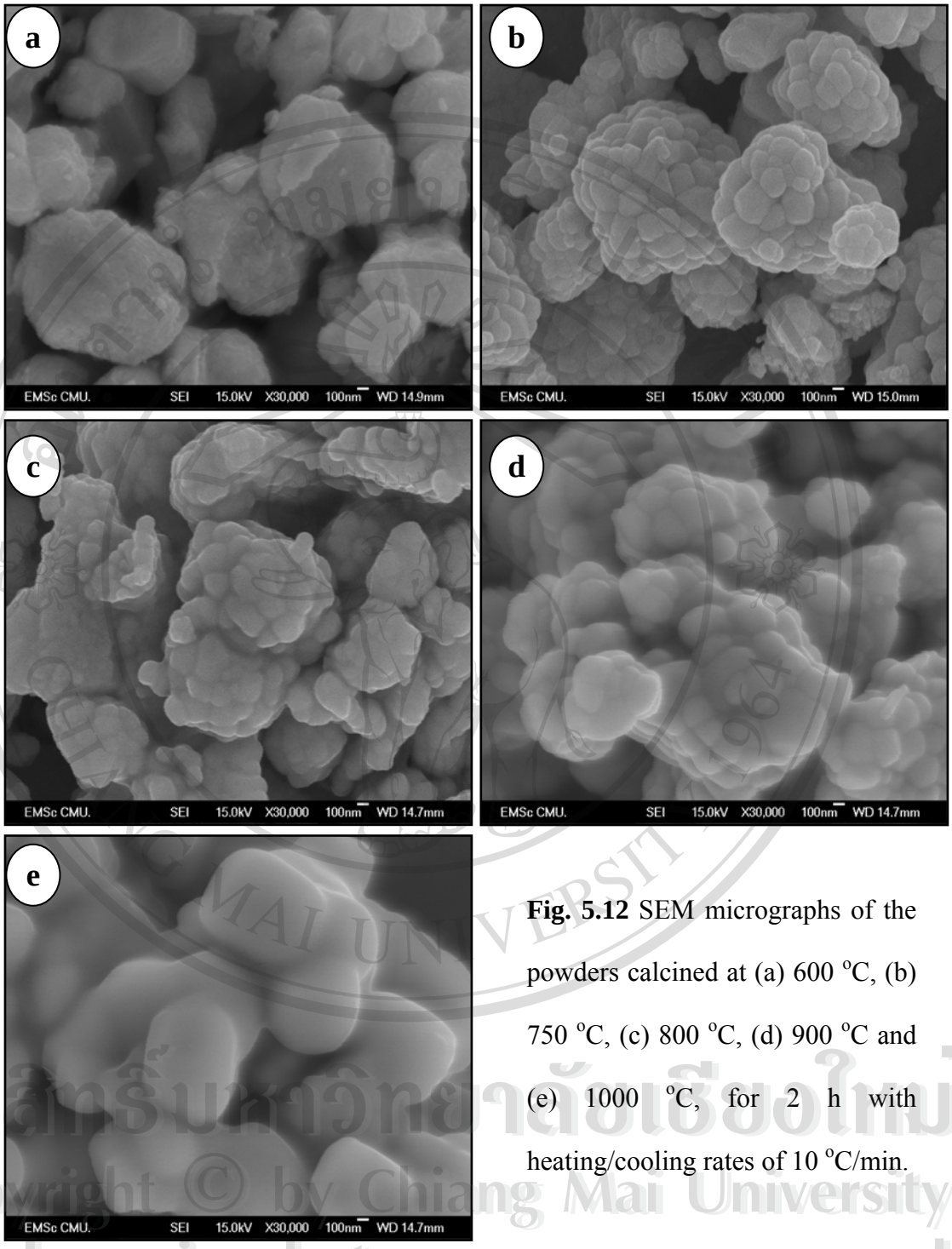


**Fig. 5.12** SEM micrographs of the powders calcined at (a) 600 $^{o}$C, (b) 750 $^{o}$C, (c) 800 $^{o}$C, (d) 900 $^{o}$C and (e) 1000 $^{o}$C, for 2 h with heating/cooling rates of 10 $^{o}$C/min.

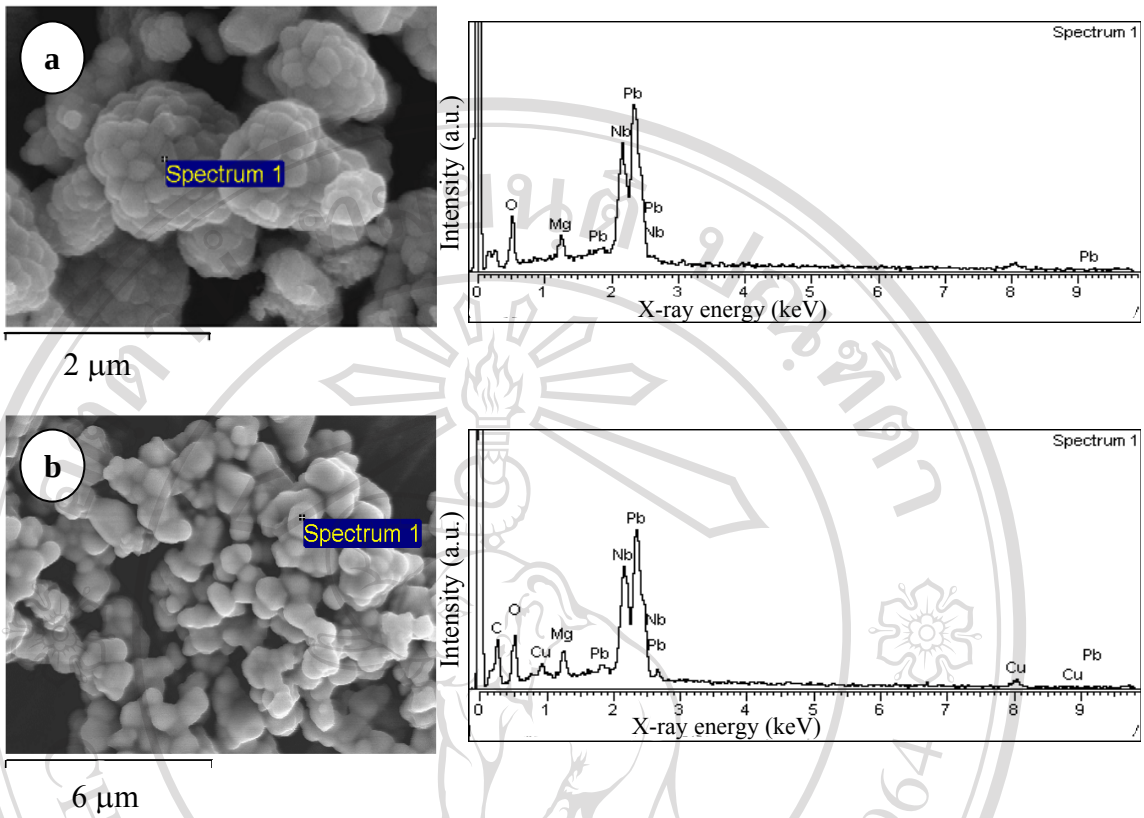


**Fig. 5.13** SEM micrographs and X-ray microanalysis spectra from the PMN powders calcined at (a) 750 $^{o}$C and (b) 1000 $^{o}$C.

**Table 5.2** Chemical compositions of the PMN powders (calcined at 750 $^{o}$C and 1000 $^{o}$C) from EDX analyser.

| Spectrum | Compositions (at %) | | | Possible phases |
|---|---|---|---|---|
| | Pb (K) | Mg (K) | Nb (M) | |
| (a) | 14.18 | 4.94 | 17.48 | $Pb_3MgNb_4O_{28}$ |
| (b) | 13.57 | 5.61 | 17.01 | $Pb_5Mg_2Nb_6O_{44}$ |

## 5.3 Lead Magnesium Niobate Ceramic

The purpose of this section is to study the phase formation, densification, microstructure and dielectric properties of sintered PMN ceramics fabricated by the pressureless sintering method, i.e. the conventional technique. Variables of the processing included deviation from the PMN stoichiometry, sintering temperature, dwell time and heating/cooling rates.

### 5.3.1 Phase Analysis

XRD patterns of PMN ceramics sintered at various temperatures are given in Fig. 5.14. The strongest reflections in the majority of the XRD patterns indicate the formation of $Pb(Mg_{1/3}Nb_{2/3})O_3$, which could be matched with JCPDS file no. 81-861.[132] To a first approximation, this phase has a cubic perovskite-type structure in space group *Pm3m* (no. 221), with cell parameters $a$ = 404.41 pm. However, some additional reflections (marked by •), which correlate with a pyrochlore phase of composition $Pb_{1.83}Mg_{0.29}Nb_{1.71}O_{6.39}$ (JCPDS file no. 33-769)[47, 133] are found in all XRD patterns. This phase has an orthorhombic structure with cell parameter $a$ = 105.9 pm in space group *Fd3m* (no. 227). This particular phase has been found in the PMN powder calcined at high temperature as reported in the previous section.

For the purpose of estimating the concentrations of pyrochlore phase present, equation (3.5) has been applied to the obtained diffraction patterns, as given in Table 5.4. It should be noted that no evidence of pyrochlore phases $Pb_2Nb_2O_7$, $Pb_5Nb_4O_{15}$, $PbNb_2O_6$, $Pb_3Nb_2O_8$, $PbNb_4O_{11}$, and $Pb_3Nb_4O_{13}$ has been found here.[57, 123] The effect of sintering temperature in the range from 1150 to1290 $^oC$ on phase formation was found to be insignificant, with no single phase of perovskite PMN obtained in all

cases. As expected, this is the reflection of unpure PMN precursor obtained from the previous section. However, the amount of PMN perovskite phase increase with increasing sintering temperatures. This may be the result of PMN ceramics being covered by PZ powders as protection for PbO volatilization.

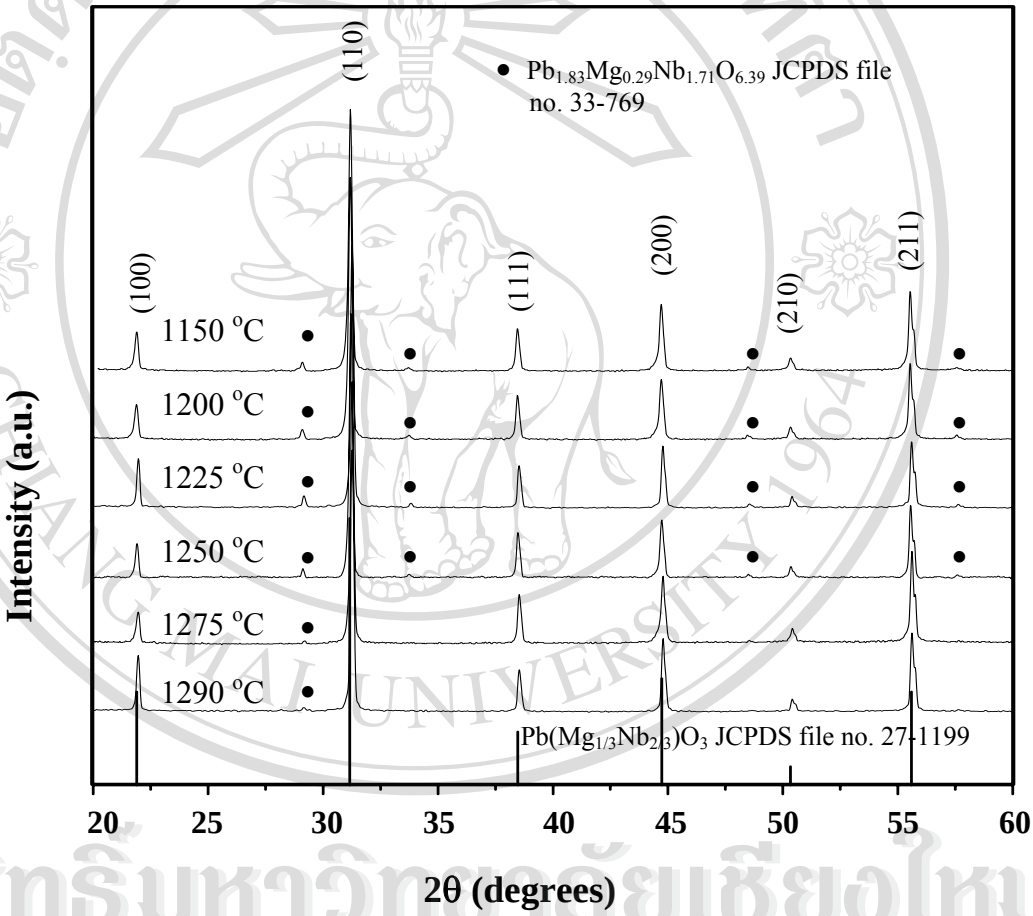


**Fig. 5.14** XRD patterns of PMN ceramics sintered at various temperatures for 4 h with heating/cooling rates of 10 °C/min.

Based on the XRD data obtained here together with the literature,[16] it may be concluded that the optimal sintering temperature for the production of PMN ceramic is 1275 $^{o}$C. In this sample it is seen that the pyrochlore phase of about 0.66 wt% was found to coexist with the perovskite phase. By employing the combination of SEM and EDX techniques, more information were obtained as shown in Fig. 5.15. EDS analysis of the facet grains (spectrum 1) indicated the chemical composition of $Pb_6(MgNb_{10})O_{32}$ or $Pb_{1.83}(Mg_{0.37}Nb_{3.06})O_{10}$. It should be noted that in this work, no unreacted MgO and PbO liquid phase have been found on the grain boundary.[16, 123, 129] This phase was mainly observed between perovskite grains (spectrum 2).

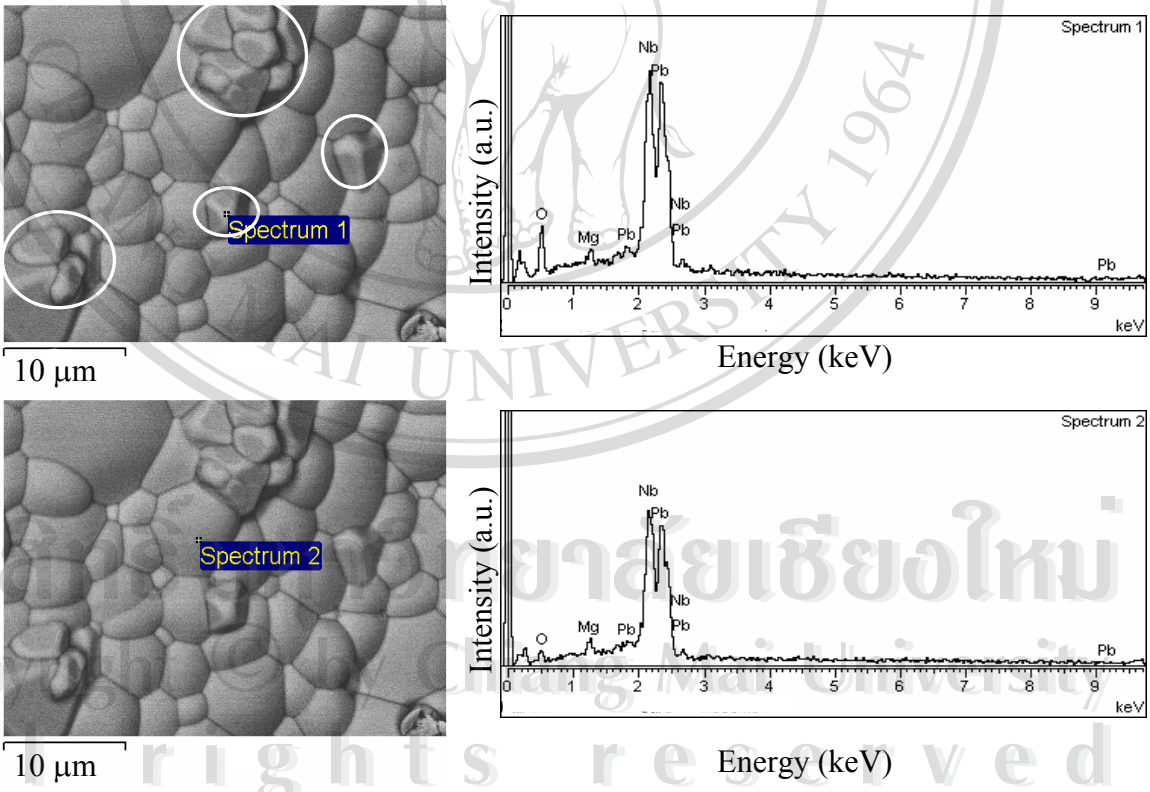


**Fig. 5.15** SEM micrographs and X-ray microanalysis spectra from different grains of PMN ceramic.

**Table 5.3** Chemical compositions of the PMN ceramics (sintered at 1250 $^{o}$C for 4 h with heating/cooling rates of 10 $^{o}$C/min) from EDX analyser.

| Spectrum | Compositions (at %) | | | Possible phases |
|---|---|---|---|---|
| | Mg (K) | Nb (L) | Pb (M) | |
| 1 | 7.17 | 58.41 | 34.76 | $Pb_6(MgNb_{10})O_{32}$ |
| 2 | 16.13 | 33.34 | 50.52 | $Pb_3(MgNb_2)O_9$ |

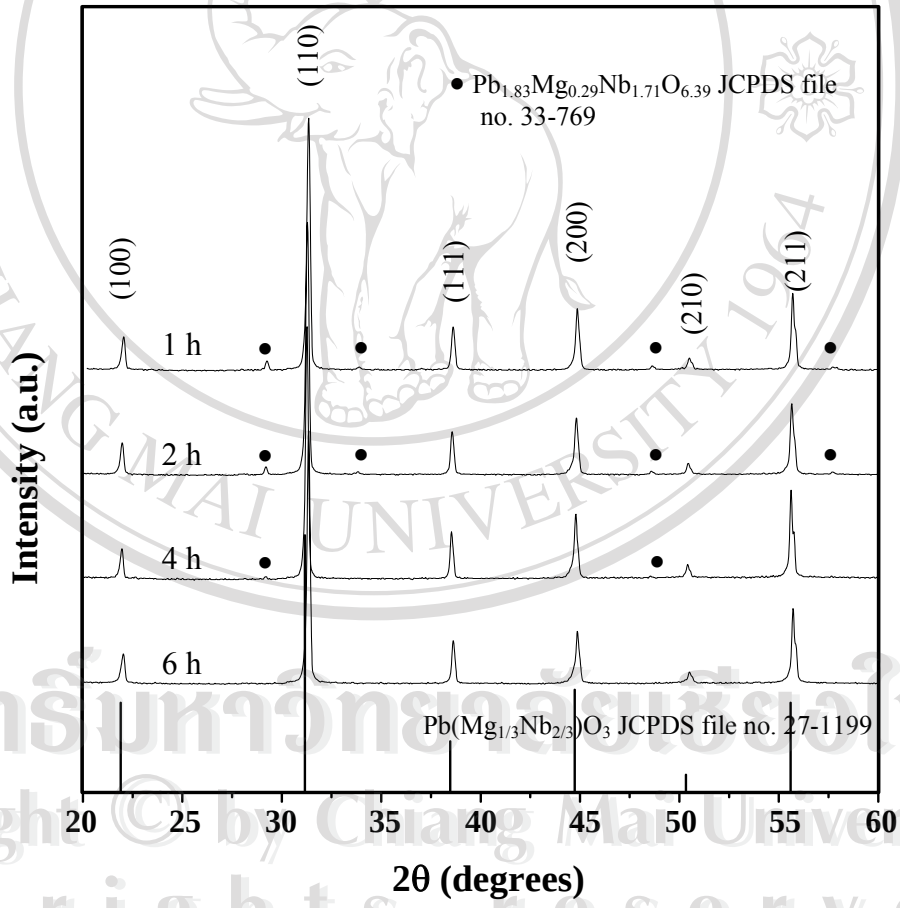




**Fig. 5.16** XRD patterns of PMN ceramics sintered at 1275 $^{o}$C with heating/cooling rates of 10 $^{o}$C/min for various dwell times.

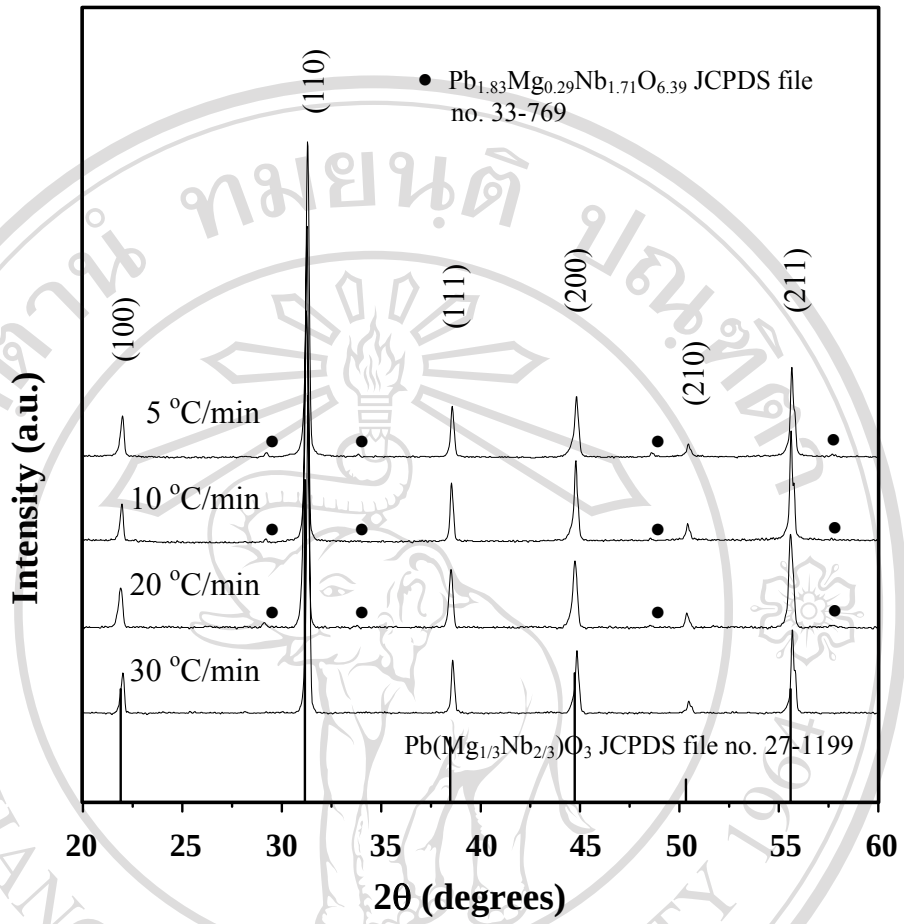


**Fig. 5.17** XRD patterns of PMN ceramics sintered at 1275 °C for 4 h with various heating/cooling rates.

Apart from the sintering temperature, the effects of dwell times (1-6 h) and heating/cooling rates (5-30 °C/min) were also found to be significant (Figs. 5.16 and 5.17). In this work, it is seen that the single phase of perovskite PMN was found to be possible only in ceramics, sintered at 1275 °C for 6 h with heating/cooling rates of 10 °C/min or 1275 °C for 4 h with heating/cooling rates of 30 °C/min.

**Table 5.4** Effect of sintering conditions on phase formation of PMN ceramics.

| Sintering Conditions | | | Qualitative concentrations of phases | |
|---|---|---|---|---|
| Sintering temperature ($^{o}$C) | Heating/cooling rates ($^{o}$C/min) | Dwell time (h) | Perovskite phase (wt%) | Pyrochlore phase (wt%) |
| 1150 | 10 | 4 | 96.76 | 3.24 |
| 1200 | 10 | 4 | 96.72 | 3.28 |
| 1225 | 10 | 4 | 9610 | 3.90 |
| 1250 | 10 | 4 | 97.37 | 2.63 |
| 1275 | 10 | 4 | 99.34 | 0.66 |
| 1290 | 10 | 4 | 98.64 | 1.36 |
| 1275 | 10 | 1 | 96.72 | 3.28 |
| 1275 | 10 | 2 | 97.05 | 2.95 |
| 1275 | 10 | 6 | 100.00 | 0.00 |
| 1275 | 5 | 4 | 98.64 | 1.63 |
| 1275 | 20 | 4 | 98.68 | 1.32 |
| 1275 | 30 | 4 | 100.00 | 0.00 |

The effect of sintering conditions on the phase formation of PMN ceramics were pronounced especially at higher temperature. Further information of PMN ceramics such as microstructure and dielectric properties from other study is needed and these will be described in the following section.

### 5.3.2 Densification and Microstructural Analysis

In this section, densification and porosity of the PMN for various sintering conditions are investigated. The relation of the densities and porosity of PMN ceramics versus the sintering temperatures are depicted in Fig. 5.18. It is observed that a density of about 78-95 % of the theoretical value for PMN can be achieved in this study. The maximum density was obtained only in the samples sintered at 1200 $^{o}$C for 4 h with heating/cooling rates of 10 $^{o}$C/min. From Fig. 5.18, the observed fall-off in density at higher temperature is probably due both to loss of PbO impeding the sintering process and the lower density of the perovskite PMN phase deformed from the $Pb_{1.83}Nb_{1.71}Mg_{0.29}O_{6.39}$ phaes, in consistent with other work.[18, 57] The effect of dwell times and heating/cooling rates on the densification of PMN ceramics are also demonstrated in Table 5.5.

Shrinkage and weight losses data of all samples sintered at various conditions are illustrated in Fig. 5.19. The change in dimension was rapidly increased with sintering temperatures at 1100 $^{o}$C to 1200 $^{o}$C and nearly constant after 1200 $^{o}$C. From these results, it is proposed that the solid-state sintering mechanism take place at temperature between 1100-1200 °C which leading to a higher density, lowest porosity and higher shrinkage. Above 1275 $^{o}$C, the linear shrinkage tends to decrease.

Weight loss data of samples sintered at temperatures from 1100 to 1320°C for 4 h which were obtained by recording the weights of the samples before and after sintering, are shown in Fig. 5.19. In general, weight loss increases with sintering temperature. However, there is a marked sensitivity of weight loss above 1150 °C (> 1%). Thus, the observed rising in weight loss after sintering process could be attributed to volatilization of Pb species. However, there is no obvious relation between weight loss and density results reported earlier.

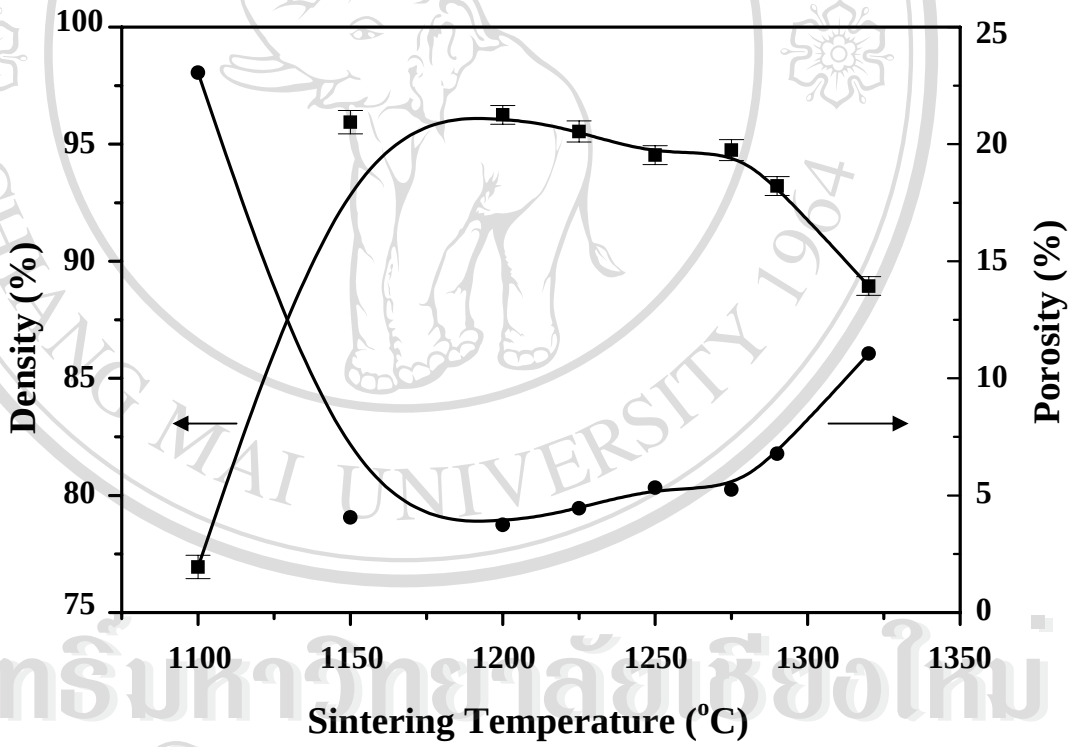




**Fig. 5.18** Variation of density and porosity with sintering temperature for PMN ceramics sintered for 4 h with heating/cooling rates of 10 °C/min.

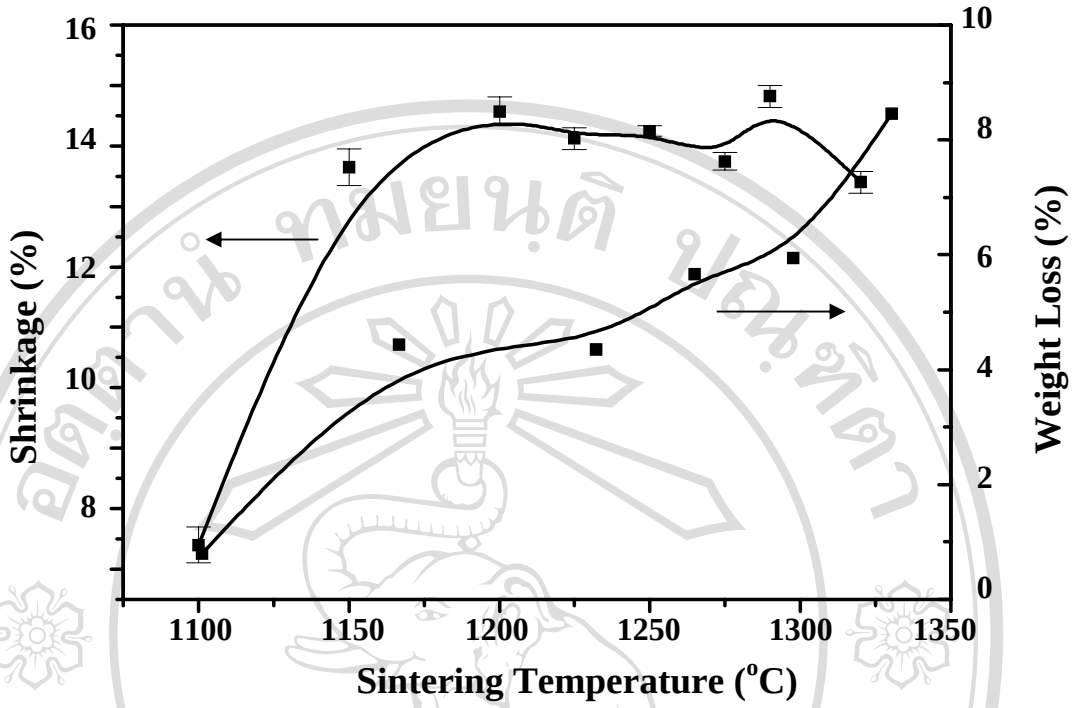


**Fig. 5.19** Dependence of shrinkage and weight loss on sintering temperature for PMN ceramics.

Free and fracture surface micrographs of PMN ceramics sintered at various conditions are shown in Figs. 5.20-5.23. In general, uniformly sized grains with a high degree of grain close-packing and rounded microstrutural characteristics of typical PMN ceramics[123, 134] are observed. The grain growth with increasing sintering temperature and dwell time are found, in consistent with Ananta et al.[126] However, at the higher sintering temperature (Fig. 5.22 (d)) and longer dwell time (Fig. 5.22 (d)), abnormal grain growth which is senn as irregular grain shape and size are detected.

**Table 5.5** Effect of sintering conditions on phase formation and densification in sintered PMN ceramics.

| Sintering conditions | | | Perovskite (wt%) | Grain size♦ (μm) | Density+ ($g/cm^3$) |
|---|---|---|---|---|---|
| Sintering ($^oC$) | Dwell time (h) | Rates ($^oC$/min) | | | |
| 1150 | 4 | 10 | 96.76 | 0.4-2.0 | 7.83 |
| 1200 | 4 | 10 | 96.72 | 0.6-3.2 | 7.86 |
| 1225 | 4 | 10 | 9610 | 1.0-5.0 | 7.80 |
| 1250 | 4 | 10 | 97.37 | 1.5-6.0 | 7.73 |
| 1275 | 4 | 10 | 99.34 | 2.0-12.0 | 7.74 |
| 1290 | 4 | 10 | 98.64 | 2.0- 14.1 | 7.61 |
| 1275 | 1 | 10 | 96.72 | 1.0-5.0 | 7.83 |
| 1275 | 2 | 10 | 97.05 | 1.2-8.1 | 7.73 |
| 1275 | 6 | 10 | 100.00 | 4.3-15.8 | 7.72 |
| 1275 | 4 | 1 | 98.62 | 2.8-14.0 | 7.69 |
| 1275 | 4 | 5 | 98.64 | 2.4-14.2 | 7.70 |
| 1275 | 4 | 20 | 98.68 | 2.0-15.6 | 7.69 |
| 1275 | 4 | 30 | 100 | 2.0-15.3 | 7.72 |

♦ The estimated precision of an average grain size is ± 0.20 μm  + The estimated precision of the density is ± 0.2 %

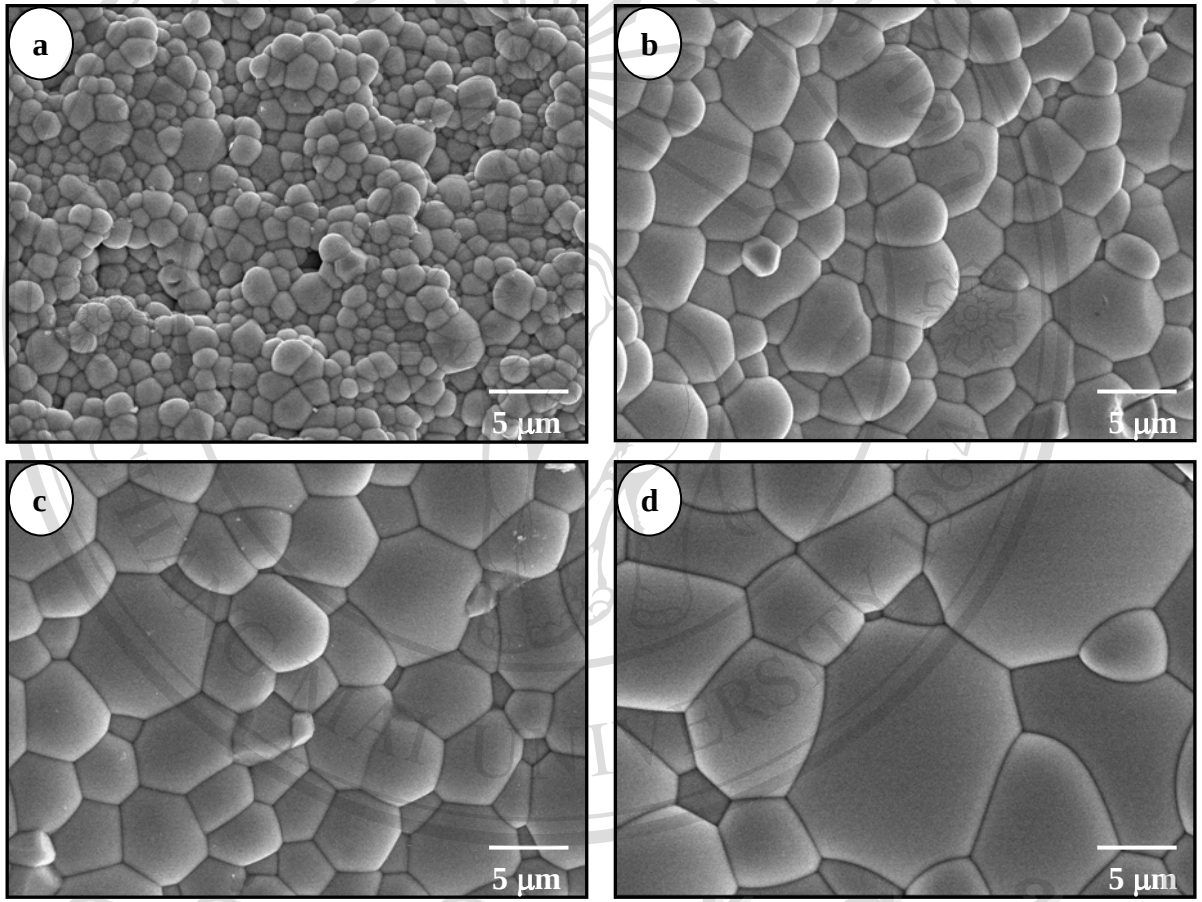


**Fig. 5.20** SEM micrographs of free surface of PMN ceramics sintered at (a) 1150 $^{o}$C, (b) 1225 $^{o}$C, (c) 1250 $^{o}$C and (d) 1275 $^{o}$C, for 4 h with heating/cooling rates of 10 $^{o}$C/min.

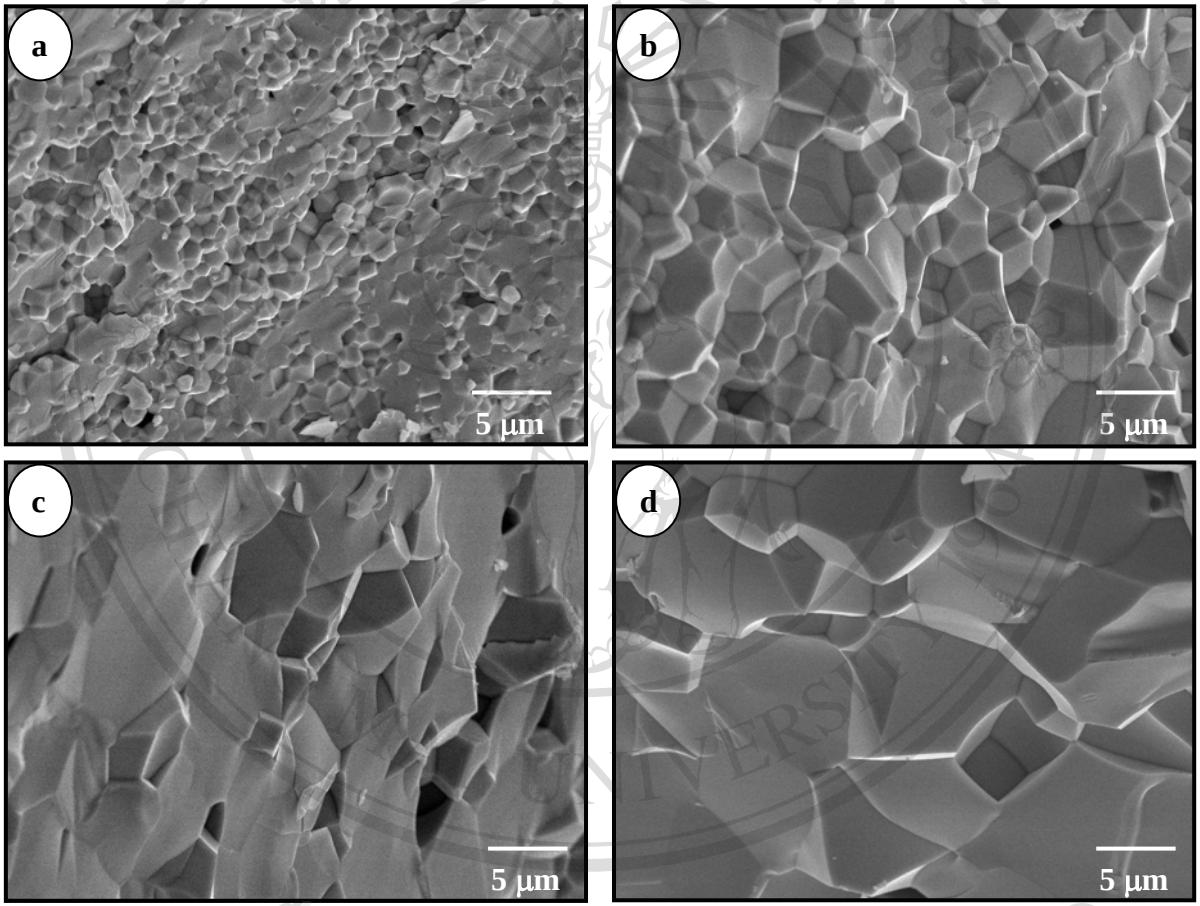


**Fig. 5.21** SEM micrographs of fracture surface of PMN ceramics sintered at (a) 1150 $^{o}$C, (b) 1225 $^{o}$C, (c) 1250 $^{o}$C and (d) 1275 $^{o}$C, for 4 h with heating/cooling rates of 10 $^{o}$C/min.

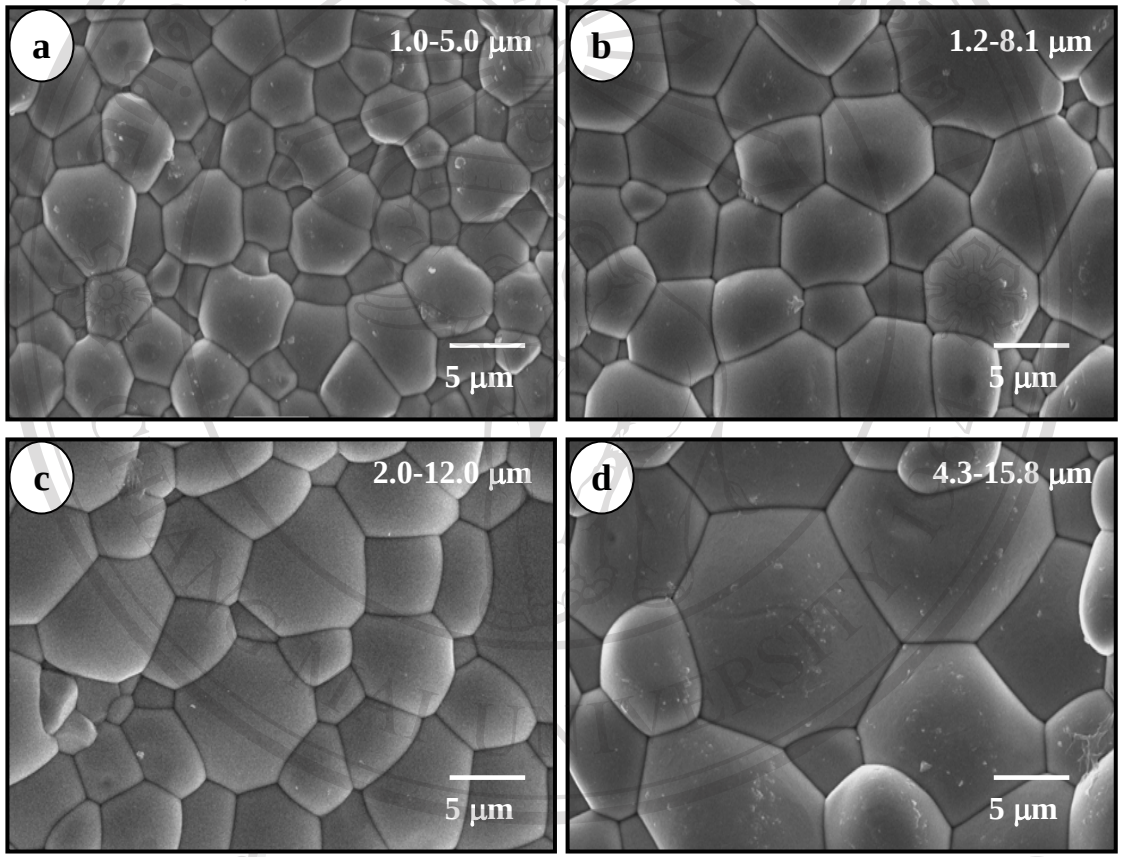


**Fig. 5.22** SEM micrographs of PMN ceramics sintered at 1275 $^{o}$C with heating/cooling rates of 10 $^{o}$C/min for (a) 1, (b) 2, (c) 4 and (d) 6 h.

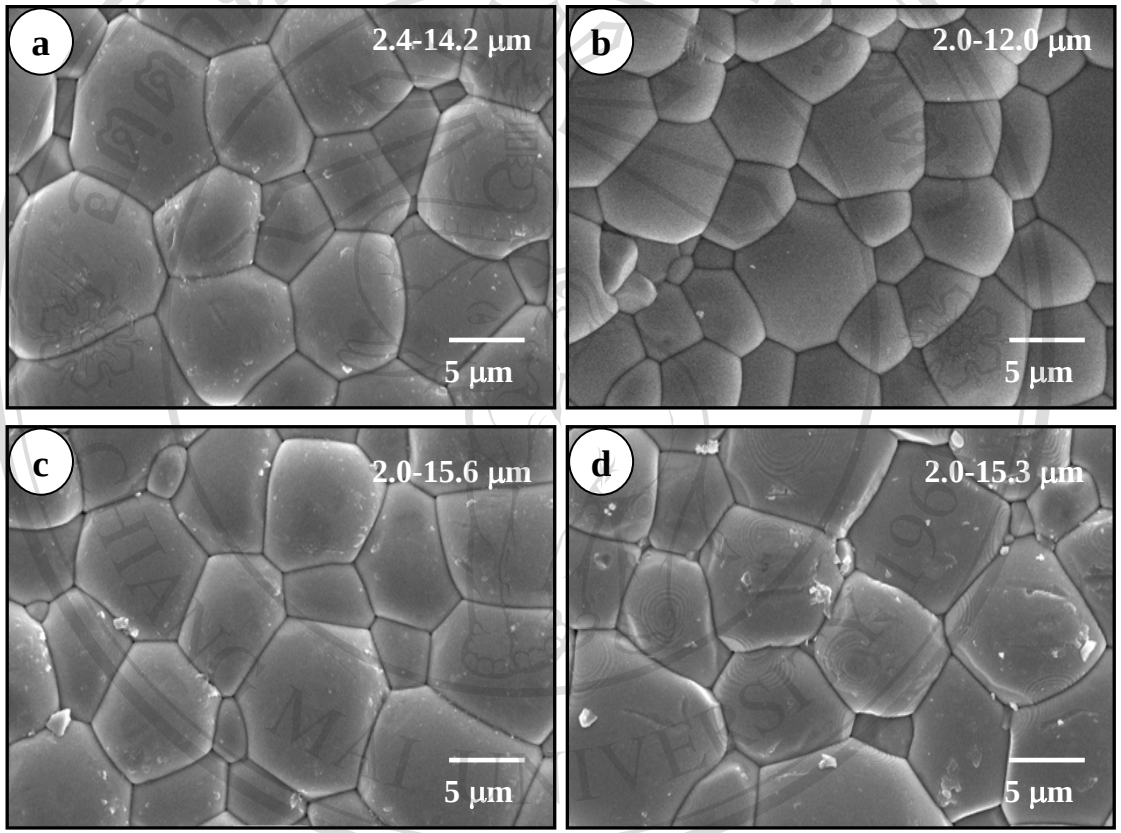


**Fig. 5.23** SEM micrographs of PMN ceramics sintered at 1275 $^{o}$C for 4 h with heating/cooling rates of (a) 5, (b) 10, (c) 20 and (d) 30$^{o}$C/min.

From Fig. 5.23, it is seen that the microstructures of PMN ceramics are relatively independent of the heating/cooling rates, at a given sintering temperature and dwell time. Secondary phases (white particles) are observed on over the grains especially at the grain boundaries (Figs. 5.23 (c) & (d)). This observation disagrees with the XRD results and could be attributed to volatilization of PbO or consequence of impure PMN starting powders.

### 5.3.3 Dielectric Properties

In order to evaluate the dielectric properties, all sintered PMN samples were measured at frequencies between 1 and 100 kHz in the temperature range from -50 to +150 $^{o}$C as shown in Fig. 5.24. The values of $\varepsilon_{r,max}$, tan $\delta_{max}$ and temperatures $T(\varepsilon_{r,max})$ and $T(\tan \delta_{max})$ obtained under different sintering temperature for the sintered PMN ceramics are given in Table 5.6. In general, the PMN samples exhibited a typical relaxor ferroelectric response, with temperatures of maximum dielectric constant, $T(\varepsilon_{r,max})$, of about -10 $^{o}$C (1 kHz), in agreement with author work.[120] In this work, it is found that magnitude of both $\varepsilon_{r,max}$ and tan $\delta_{max}$ in sintered PMN samples depends considerably upon the sintering conditions. The results are consistent with earlier work on other PMN-based systems.[126, 135]

In Fig. 5.24 and Table 5.6, the maximum dielectric constant value of PMN ceramics remarkably increases from 10073 to 16546 as the sintering temperature rises from 1150 to 1200 $^{o}$C, then gradually decreases to 12984 at sintering temperature of 1275 $^{o}$C. This trend is similar to that reported in the literature.[126]

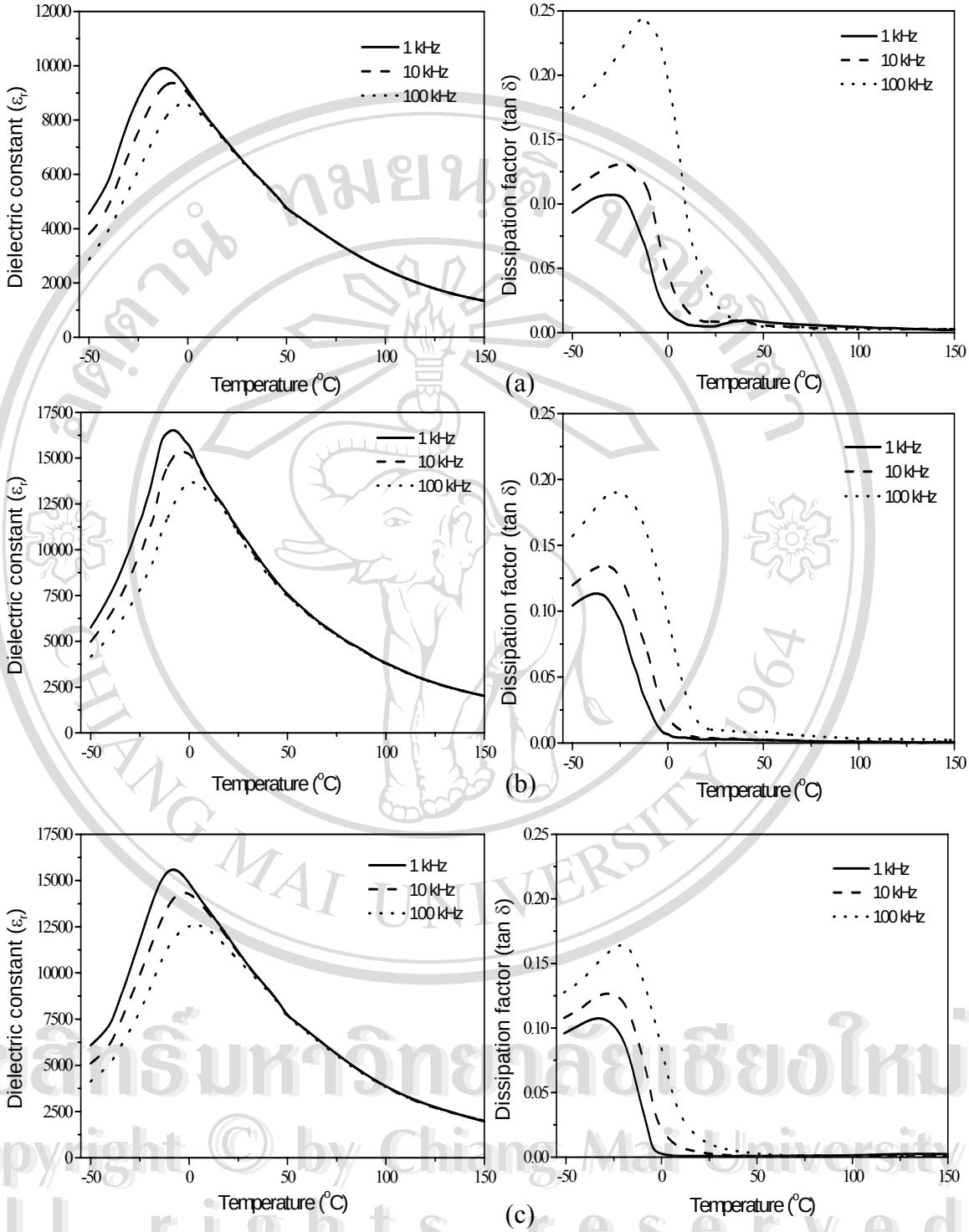


**Fig. 5.24** Dielectric constant and dissipation factor of PMN ceramics sintered at (a) 1150 °C, (b) 1200 °C, (c) 1225 °C, (d) 1250 °C and (e) 1275 °C, for 4 h with heating/cooling rates of 10 °C/min.

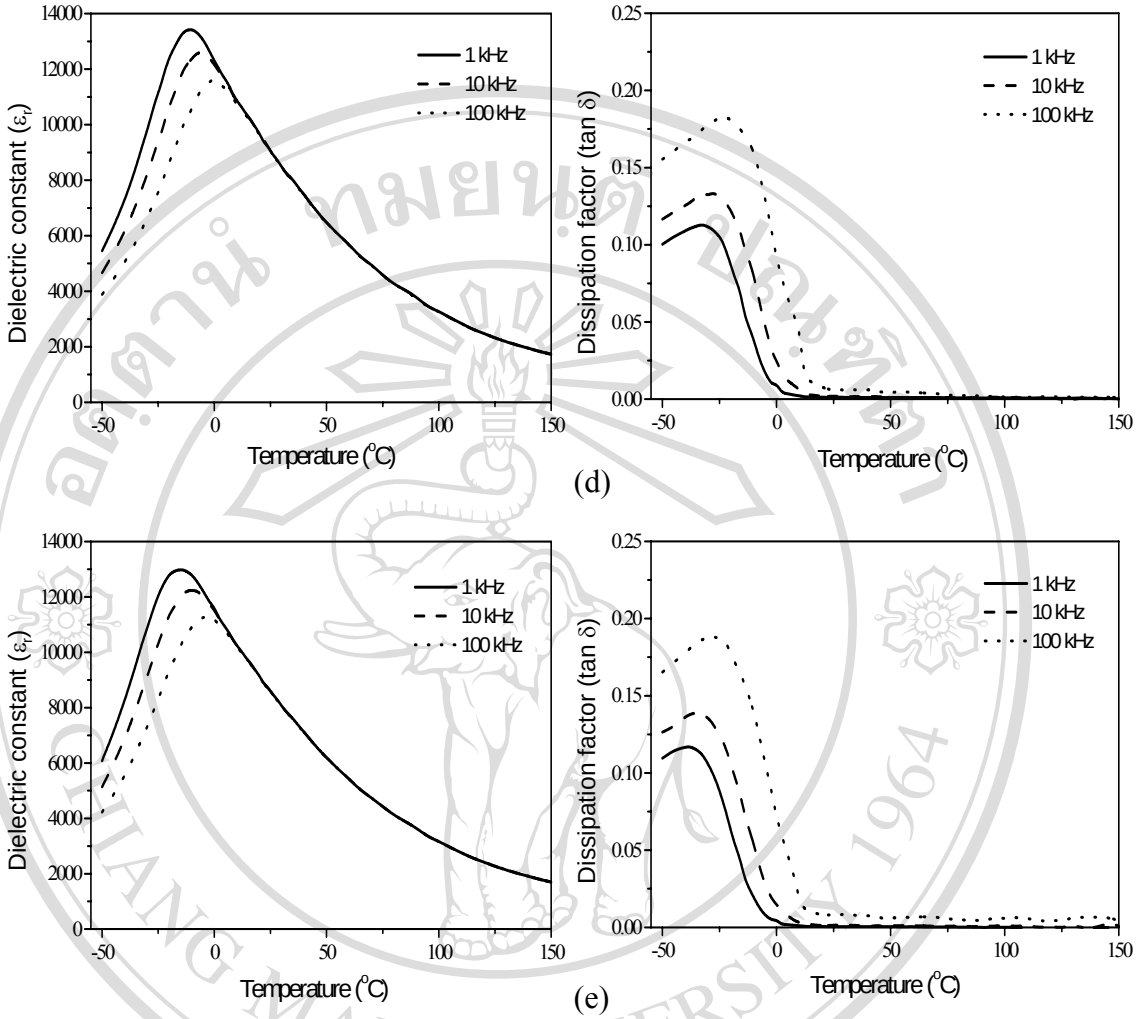


**Fig. 5.24** (Continued)

**Table 5.6** Physical and dielectric properties of PMN ceramics sintered at various temperatures for 4 h with heating/cooling rates of 10 $^{o}$C/min.

| Sintering temperature ($^{o}$C) | $T(\varepsilon_{r,max})$ ($^{o}$C) | 1 kHz | | | | |
|---|---|---|---|---|---|---|
| | | $\varepsilon_r(T_R)$ | tan $\delta$ ($T_R$) | $\varepsilon_{r,max}$ | tan $\delta_{max}$ | Average grain size (μm) |
| 1150 | -8 | 6593 | 0.0028 | 10073 | 0.1071 | 1.00 |
| 1200 | -8 | 10403 | 0.0108 | 16546 | 0.1071 | 1.69 |
| 1225 | -8 | 10905 | 0.0060 | 15949 | 0.1132 | 3.73 |
| 1250 | -10 | 8919 | 0.0013 | 13429 | 0.1126 | 6.01 |
| 1275 | -14 | 8478 | 0.0005 | 12984 | 0.1166 | 9.19 |

The variation of the dielectric constant and dissipation factor at room temperature measured at 1 kHz as a function of average grain size for PMN ceramics is shown in Fig. 5.25. At the average grain size ranging from 1-4 μm, the dielectric constant at room temperature increases as the average grain size of PMN ceramics increases. As the average grain size approaches ~ 4 μm (larger than that of PZT case), the dielectric constant becomes maximum ($\varepsilon_r$ ~ 10905). With further increase in grain size, the dielectric constant drops significantly. Similar characteristic is also observed for the dissipation factor at room temperature where maximum value of tan δ (~ 0.0108) was found at the average grain size ~ 1.69 μm.

Grain size dependence of the maximum dielectric constant and its corresponding temperature at 1 kHz for PMN ceramics is shown in Fig. 5.26. Except at the average grain size of 1 μm, the maximum dielectric constant tends to decrease as the average grain size increases. It is to be noted that there is no obvious interpretation of these relationships, although it is likely to correspond to an internal stress and domain wall mechanism proposed by a number of workers.[52, 135]

Based on this investigations, it is believed that microstructural dependency on the dielectric properties is not expected in PMN ceramics since the underlying phenomena associated with relaxor ferroelectric behaviour is on the order of ~ 10 nm [136]. Observed grain size effects in PMN ceramics may be also attributed to a low dielectric constant grain boundary phases which suppress the final dielectric properties of the products.

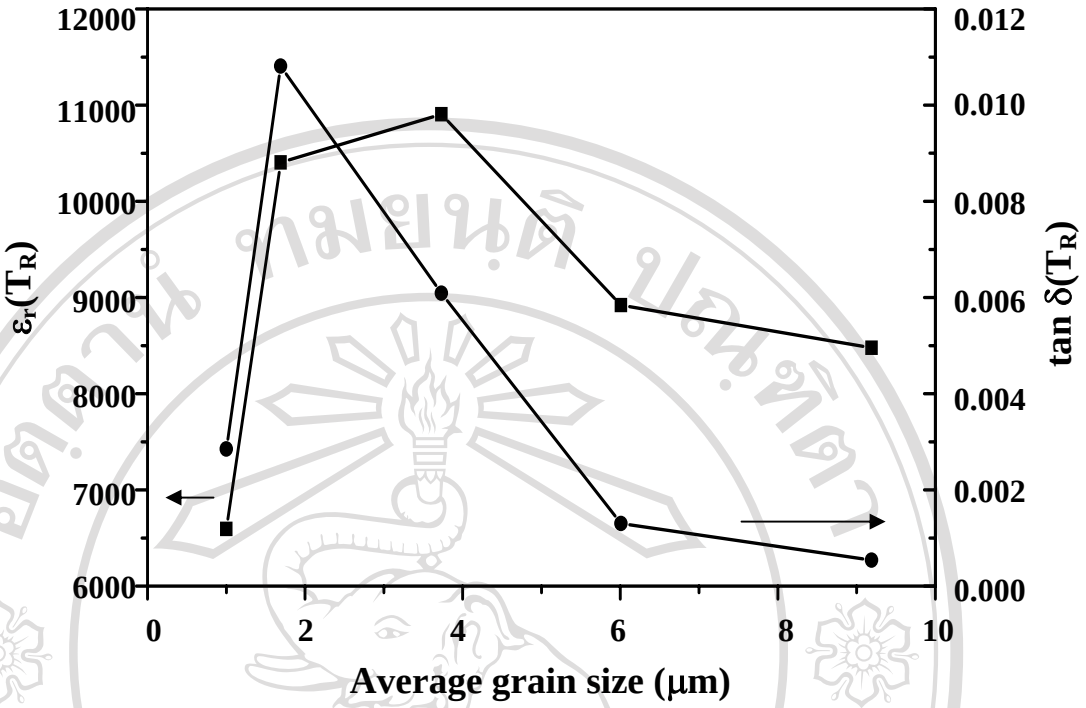


**Fig. 5.25** The average grain size versus the dielectric constant and dissipation factor at room temperature of PMN ceramics.

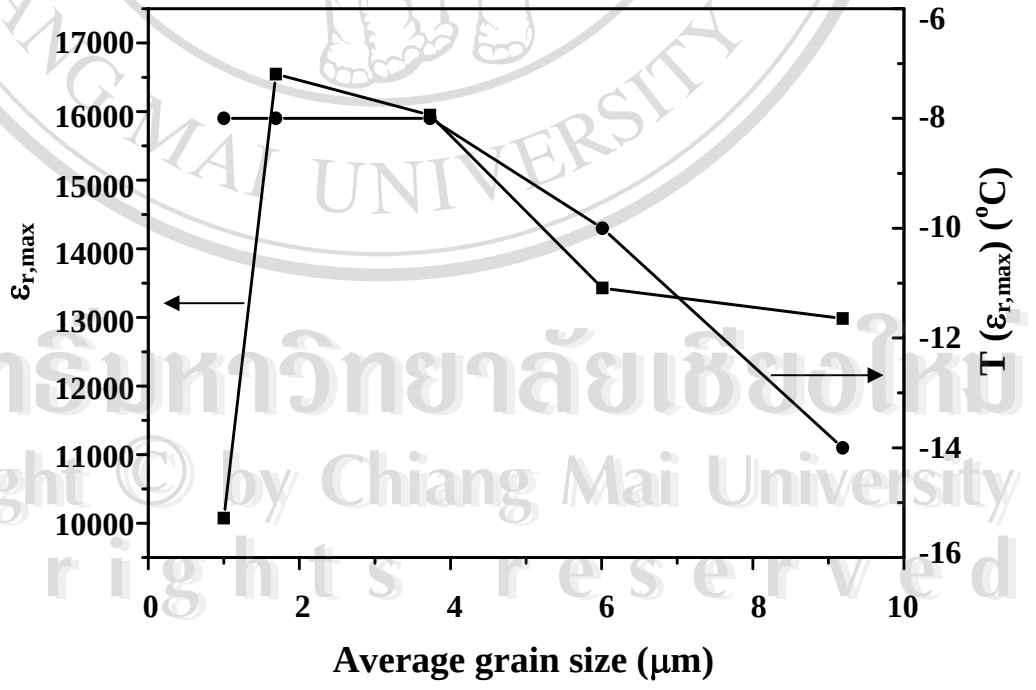


**Fig. 5.26** The average grain size versus the maximum dielectric constant and T($\varepsilon_{r,max}$) of PMN ceramics.